E. Kereskényi et al. Journal of Archaeological Science: Reports 32 (2020) 102437

Archaeometrical results related to Neolithic amphibolite stone implements from Northeast Hungary

Erika Kereskényi[a], György Szakmány[b], Béla Fehér[a], Ildikó Harsányi[c], Veronika Szilágyi[c], Zsolt Kasztovszky[c], Tivadar M. Tóth[d]

[a]Department of Mineralogy of Herman Ottó Museum, Kossuth u. 13, H-3525 Miskolc, Hungary

[b]Department of Petrology and Geochemistry, Eötvös Loránd University, Pázmány Péter sétány 1/c, H-1117 Budapest, Hungary

[c]Nuclear Analysis and Radiography Department, Centre for Energy Research, PO Box 49, H-1525 Budapest 114, Hungary

[d]Department of Mineralogy, Geochemistry and Petrology, University of Szeged, Egyetem u. 2, H-6722 Szeged, Hungary

Abstract: 28 amphibolite Neolithic polished stone implements deriving from different archaeological localities and cultures in Northeast Hungary (Borsod-Abaúj-Zemplén County) were archaeometrically analysed by mainly non-destructive methods (MS, EDS/SEM, PGAA). Bulk chemistry of the samples showing subalkali characteristics. The amphibolite polished stone tools were divided into two groups based on their mineral components and metamorphic evolution. A single Ca-amphibole approach was used to calculate peak P-T conditions to determine a thermobarometric model for the amphibolite implements. Data of the studied samples were compared to those of the nearest amphibolite outcrops in Gemericum, Veporicum, Tatricum and Zemplinikum (Slovakia). The Variscan P-T loop covered the thermobarometric data of the analysed stone implements and the amphibolite outcrops. The source areas are assumed to be these fields and/or the crossing riverbeds flowing through them to Borsod-Abaúj-Zemplén County, the archaeological collecting territory of the amphibolite stone axes.

Keywords: amphibolite, polished stone tools, provenance field, Neolithic, Hungary

Mineral abbreviations: A*mp*: amphibole; M*g-hb*: magnesio-hornblende; *Mg-f-hb*: magnesio-ferri-hornblende; F*hb*: Ferro-hornblende; *Act*: actinolite; F*act*: ferro-actinolite; S*dg:* sadanagaite; F*sdg*: ferro-sadanagaite; *Tsch*: tschermakite; F*e2-ftsch*: Ferro-ferri-tschermakite; *ftsch*: Ferro-tschermakite; *f3-ts*: Ferri-Tschermakite; P*rg*: pargasite; F*prg*: ferro-pargasite; a*ug*: Augite; D*i*: diopside; C*px:* clinopyroxene; A*b*: albite; O*lg*: oligoclase; *And*: andesine; L*ab*: labradorite; B*yt*: bytownite; Pl: plagioclase; K*fs:* K-feldspar; E*p*: epidote; C*zo*: clinozoisite; C*hl*: chlorite; B*i*: biotite; *Ms*: muscovite; P*h*: phengite; *Qtz*: quartz; T*tn*: titanite; *Ilm*: ilmenite; M*gt*: magnetite; *Ap*: hydroxylapatite; P*y*: pyrite; C*al*: calcite. Jrs: jarosite.

1. Introduction

In this paper we present the results of an archaeometrical research program on the polished stone implement collection of the Herman Ottó Museum in Hungary which started in 2014. The collecting area covers Borsod-Abaúj-Zemplén County in Northeast Hungary. The museum owns approximately 500 Neolithic polished stone implements, most of which are metabasites or more specifically in some cases blueschists (Kereskényi et al., 2018), but a significant number of volcanic and sedimentary stone implements are possessed as well according to our observations. Until now 28 tools have been shown to be made of amphibolite. Stone tools which are reached and characterized by the amphibolite facies assemblage; hornblende and plagioclase feldspar, were classified as amphibolite. Contact metamorphosed metabasites are not included among these lithotypes.

The archaeological localities where these amphibolite polished stone tools were found are shown in Fig. 1. Most of the findings have an archaeological context, but 10 of the axes were stray finds (Table 1). Borsod/Derékegyháza (Edelény) and Szerencs/Taktaföldvár are the sites with the two largest sets of finds. The Borsod/Derékegyháza (Edelény) locality belongs to the Middle Neolithic Bükk culture (Kalicz & Makkay, 1977). The Szerencs/Taktaföldvár locality represents the late Neolithic Tisza culture (Selján, 2005). Tiszadorogma (Kalicz and Makkay, 1977) and Tiszavalk/Kenderföldek are related to the Alföld Linear Pottery culture (Csengeri, 2013). Findings from Szirmabesenyő and its vicinity (Kalicz and Makkay, 1977) and Miskolc/Aldi2 are linked to the Bükk or Alföld Linear Pottery cultures (Csengeri, 2011). The Hejőkürt/Lidl locality is related to the early Tiszadob culture (Csengeri, 2015). The Emőd locality belongs to one or more of the Alföld Linear Pottery, Tiszadob, Tiszadob-Bükk or Bükk cultures according to the related ceramics (Csengeri, 2013) (Table 1).

As regards the raw materials, amphibolite and amphibolite-greenschist stone tools are abundant implements in the Neolithic and Aeneolithic periods (Hovorka et al., 2001, Méres et al., 2001, Přichystal, 2013), being described as common and often used raw materials due to flexibility and elasticity of the ready-made items because of the needle-like of amphiboles (Hovorka et al., 2001).

The most probable amphibolite source localities are not too far from the archaeological sites in the Western Carpathians. The Western Carpathians are defined by three major geological units: Veporicum, Gemericum and Tatricum (Plašienka et al., 1997). In the Veporicum, amphibolites are not dominant, but some large bodies are exposed in the Čierna Hora and the Branisko Mountains (Faryad, 1999, Faryad et al., 1999, 2005, Faryad & Jacko, 2002). Furthermore, the LAC (Leptynit-Amphibolite Complex) outcrops in Veľký Zelený stream and in Čierny Balog (Putiš et al., 1997). The Gneiss-Amphibolite Complex (GAC) in the Gemericum has two main outcrops in Rudňany (Radvanec et al., 2017) and in Klátov (Faryad, 1990, 1999, Faryad and Spišiak, 1999). The Ochtiná group is an exposure of amphibolite rocks at the contact zone of Veporicum and Gemericum (Novotná et al., 2015). There are only distant, minor occurrences in the Tatricum (Ivan et al., 2001). The most extensive outcrops are in the Tribeč Mountains (Faryad, 1999) and Little Carpathians (Ivan et al., 2001). Zemplinicum is the closest geological unit of the

Carpathians to the archaeological localities; but here the amount of amphibolites is much less than in the above regions (Faryad, 1995, Faryad and Vozárová, 1997). The vicinities of major riverbeds of Slovakia which cross Hungary cannot be excluded as possible provenance fields (Fig. 2).

In the southwestern part of Slovakia, at the Bajč archaeological site, a large number of polished stone tools were excavated with various types of amphibolite and greenschist stone axes. According to Hovorka and Cheben (1997), the possible provenance field of these amphibolites can be the Little Carpathians, Slovak Ore Mountains, Tribeč Mountains, the eastern part of the Bohemian Massif, Eastern/Northern Alps and also pebbles of the Hron and Danube riverbeds.

In this research we provide petrological and mineralogical data of the Neolithic amphibolite implements and compare them with the former published data of nearby Slovakian amphibolite source localities and specification of the most probable provenance of the raw material.

2. Analytical techniques and materials

In addition to macroscopic and stereomicroscopic descriptions, the magnetic susceptibilities of all the axes were measured by a KT-5 Kappameter, using thickness correction (Bradák et al., 2009, Szakmány et al., 2011b, Kereskényi et al., 2015 a, b.).

Non-destructive methods were applied since most of the implements are intact. While destructive analyses were performed only on some broken stone implements (Table 1).

The chemical elements in the bulk material of 24 polished archaeological stone objects (Table 1) have been measured by the prompt-gamma activation analysis (PGAA) system of the Budapest Neutron Centre. The present state of the PGAA facility in Budapest was described by Szentmiklósi et al. (2010) in detail. During the analysis, the entire objects were placed in a horizontal beam of cold neutrons guided from the Reactor. The flux of the cold neutron beam equivalent to the thermal beam was 1.2×10^8 neutrons cm^{-2} s^{-1}. During the experiments, the beam was setup to 24 mm^2 and 44 mm^2 size cross-section. With such beam collimation, the obtained count rate proved to be optimal from spectroscopic points. Since neutrons can travel into the deepest parts of the investigated object, the obtained composition data represents the bulk. Promptly after the neutron absorption, characteristic gamma radiation is emitted, which was detected with a HPGe-BGO detector system. The spectra were collected with a 36,000-channel analyser. To identify characteristic gamma lines, our PGAA library has been used. The quantitative elemental compositions have been calculated based on the k_0-method (Révay, 2009). In silicates, the PGAA method allows to determine all the major elements and some geochemically important traces (such as B, Cl, Sc, V, Cr, Co, Nd, Sm and Gd), non-destructively, see Kasztovszky et al. (2008), Szakmány and Kasztovszky (2004), and Szakmány et al. (2011a). In these experiments, the spectrum acquisition has been performed for 1200 s -3000 s, to gain enough counts in the relevant spectrum peaks to produce statistically reliable results.

Quantitative chemical spot analyses on the mineral phases were performed applying a JEOL JXA 8600 Superprobe electron-microprobe in energy-dispersive mode (EDS/SEM) at the Institute of Mineralogy and Geology, University of Miskolc. The operating conditions were as follows: accelerating voltage 15 kV, probe current 20 nA, and a 1-5 µm beam diameter. The intact tools were analysed on their original surfaces using the method of Bendő et al. (2013), while polished surface sections were made from the broken implements for their analyses (Table 1).

3. Results

3.1. Macroscopic description and magnetic susceptibility

Most of the stone implements are intact and having traces of use. They are 4.0-11.5 cm long, 1.0-6.5 cm wide and 0.5-4.0 cm thick. Regarding their archaeological typology, most of them are flat axes and chisels, but axes D21, D32, D39 have shoe-last form, D38 and D40 are shaft drilled stone axes, and D48 is a tongue-shaped axe.

Macroscopically the tools are fine-grained, compact, dominantly foliated, having grey, greyish black, greyish green and dark brown colour. Green and brown patches and bands can be recognized by naked eye.

Magnetic susceptibility values show a homogenous distribution from 0.31-0.85*10^{-3} SI. 4 samples appear from 1.44-1.77*10^{-3} SI and sporadically a continuous upward from 6.47 to 46.7*10^{-3} SI (Table 1).

3.2. Bulk rock chemistry

Bulk compositional data analysed by PGAA for the amphibolite implements are listed in Table 2. The tools are characterized by SiO_2 content ranging from 46.55 to 59.00 wt%. Sample D12 has an elevated TiO_2 content= 3.70 wt% and remarkably differs in some of the trace elements from the other analysed samples. Representing the data in a TAS diagram, the analysed samples plot in the basalt, trachybasalt, basaltic andesite and andesite fields, having subalkaline characteristics since the Na_2O+K_2O content varies between 0.92-5.17 wt%. (Fig. 3). In the AFM diagram most of the samples show tholeiitic affinity (Fig. 4).

3.3. Petrography and mineral chemistry

A total of 22 polished stone tools were analysed by EDS/SEM. Eight of them are intact stone axes and were analysed by the “original surface” method (Bendő et al., 2013). In these cases, the zoned mineralogical features (e.g. the existence of tiny or scarce phases) the zonation of the amphiboles could not always be perceived.

Most of the stone implements are fine-grained, but some stone tools (D08, D12, D13, D15, D18 and D30 are coarse-grained (Figs. 5 A—D, 6 A—C). Most of the axes are foliated (Figs. 7 A—D) except B04, B05, B12, D17, D18, D33, D45 and D47 samples.

The amphibolites consist mainly of Ca-amphibole (Mg-hb, Act, Tsch, Prg, Sdg), plagioclase, epidote, clinozoisite, chlorite and quartz. Some samples contain clinopyroxene, K-feldspar, biotite in minor quantity. Titanite and ilmenite are abundant accessory minerals (Table 3).

According to the textural relations, chemical compositions and the assemblage of coexisting phases, two varieties of the detected stone implements can be distinguished. The first variety (*Group1*) includes six samples and it consists of Ca-amphiboles with increasing Al(tot) content from cores to rims. Actinolite and magnesio-hornblende are preserved in the cores with Al(tot) 0.14-2.84 apfu (atoms per formula unit), while at the rims magnesio-hornblende, pargasite and tschermakite have crystallized with Al(tot) 0.73-2.83 apfu (Fig. 8).

The second group (*Group2*) includes 16 pieces of stone tools and their amphibole content corresponds to hornblende, pargasite, tschermakite and sadanagaite in the core with actinolite at the rims, just the opposite of the order in Group1 tools. Group2 was divided into four subgroups based on mineral associations:

- *Group2a* includes most of the implements in which no K-feldspar or biotite were detected (B12, D02, D04, D08, D18, D21, D32, D47),
- K-feldspar±biotite-bearing amphibolites (*Group2b*: B04, B05, C02, D48),
- Clinopyroxene±biotite-bearing amphibolites (*Group2c*: D15, D34, D45),
- Biotite-bearing amphibolite without K-feldspar and clinopyroxene (*Group2d*: D17).

3.3.1. Amphibole

The ACES Excel spreadsheet was used to calculate cation numbers of amphiboles. Since the Fe^{3+}/Fe(tot) ratio cannot be measured by electron-microprobe, the smallest maximum deviations criteria were applied for adjusting the valences of Fe by automatically selecting one or more of four cation normalization schemes: sum Si to Ca (+Li) = 15; sum Si to Mg (+Li) = 13; sum Si to Na = 15; and sum Si to K = 16 apfu (Locock, 2014). Applied amphibole nomenclature corresponds to the recent IMA rules (Hawthorne et al., 2012).

Group1

In each detected commonly zoned Ca-amphibole of the *Group1* variety, the ^{B}Na/(Ca+Na) varies in a narrow range of 0.00-0.19 both in the cores and rims. Overlapping ^{A}Na and X_{Mg} values characterize amphiboles in the cores and at the rims. ^{A}Na ranges over 0.00-0.65 apfu and X_{Mg} is fairly homogenous with values of 0.49-0.79.

Actinolite with ^{IV}Al 0.12-0.44, ^{VI}Al 0.01-0.65 and Al(tot) 0.14-1.03 apfu was detected in the cores of all samples except D30. Magnesio-hornblende occurs in the cores of the D05, D30 and D31 samples with ^{IV}Al 0.33-1.13, ^{VI}Al 0.50-1.71, Al(tot) 0.44-2.84 apfu. In the D05, D12, D13 and D33 samples, magnesio-hornblende–magnesio-ferri-hornblende with ^{IV}Al 0.28-1.12, ^{VI}Al 0.60-1.64 and Al(tot) 0.73-2.75 apfu makes a rim of actinolite-magnesio-hornblende (Fig. 5 B, D). Tschermakite was detected at the rims of earlier crystallized amphiboles in D05, D30 and D31 samples with ^{IV}Al 1.10-1.48, ^{VI}Al 1.15-1.55 and Al(tot) 2.50-2.63. Pargasite with ^{IV}Al 0.72-1.13, ^{VI}Al 1.52-1.70, Al(tot) 2.31-2.83 apfu was described from the rims on the actinolite–magnesio-hornblende in the D30 and D31 samples.

Group2

In *Group2* the ^{A}Na values are 0.00-0.60 apfu, ^{B}Na/(Ca+Na) ranges from 0.00 to 0.19 and X_{Mg} is 0.30-0.79, values which overlap in the cores and rims.

Generally, in *Group2a* (Figs. 6 G—I, Fig. 7 D) most of the samples have a magnesio-hornblende core with ^{IV}Al 0.01-0.93, ^{VI}Al 0.07-1.79, Al(tot) 0.84-2.29 apfu, and actinolite–hornblende was observed with ^{IV}Al 0.18-0.54, ^{VI}Al 0.00-0.50, Al(tot) 0.23-0.89 apfu at the rims. Ferri-tschermakite and ferro-ferri-tschermakite were determined for the core of sample D08 (Fig. 7 C—D) with Al(tot) 2.13 apfu. In the core of the D47 stone implement pargasite–ferropargasite prevail with Al(tot) 2.64-3.31 apfu in addition to magnesio-hornblende. In the core of the B12 tool pargasite, ferropargasite, sadanagaite and ferrosadanagaite (Fig. 6—I) are present with an increased Al(tot) from 2.97 to 3.45 apfu.

In *Group2b* most of the samples have magnesio-hornblende–ferro-hornblende cores, although in D48 pargasite and ferro-pargasite were detected also. The amphibole cores have ranges of ^{IV}Al 0.41-0.75, ^{VI}Al 0.39-1.40, Al(tot) 0.86-2.00 apfu, while at the actinolite rims a significant decrease shows up, with ranges of ^{IV}Al 0.23-0.48, ^{VI}Al 0-0.42, Al(tot) 0.36-0.66 apfu.

In *Group2c* magnesio-hornblende–ferro-hornblende cores were recorded having ^{IV}Al 0.30-0.92, ^{VI}Al 0.60-1.30, Al(tot) 0.83-2.21 apfu and at the rims magnesio-hornblende–actinolite were observed with ^{IV}Al 0.07-0.35, ^{VI}Al 0.27-0.64, Al(tot) 0.52-1.03 apfu.

Group2d consists of only the D17 implement, in which magnesio-hornblende–ferropargasite exists in the core with ^{IV}Al 0.35-1.03, ^{VI}Al 0.39-1.68 Al(tot) 0.86-2.73 apfu and with magnesio-hornblende–actinolite rimming the earlier crystallized amphiboles with ^{IV}Al 0.13-0.42, ^{VI}Al 0.05-0.43, Al(tot) 0.18-0.76 apfu.

Chemical compositions of the calcic amphiboles are presented in Tables 4, 5.

The detected amphiboles of the amphibolites of *Group1* and *Group2* lie in the actinolite, magnesio-hornblende, tschermakite, pargasite, and sadanagaite fields (Figs. 8, 9) in the ^{A}(Na+K+2Ca) vs ^{C}(Al+Fe^{3+}+2Ti) diagrams.

3.3.2 Pyroxenes

The pyroxene formula was calculated on the basis of 6 oxygens. The FeO/Fe_2O_3 ratio was estimated assuming a total number of cations of 4. Normalized pyroxene end members found in amphibolites are plotted in the En-Fs-Wo diagram (Fig. 10) of Morimoto (1989). *Augite* forms hypidioblasts and xenoblasts as a relict phase next to actinolite and hornblende in small amounts in the D34 ($En_{0.37}$ $Fs_{0.28}$ $Wo_{0.34}$) and D45 samples ($En_{0.28\text{-}0.39}$ $Fs_{0.25\text{-}0.50}$ $Wo_{0.23\text{-}0.42}$). *Diopside* is observed as a relict phase in the D15 sample. Its chemical composition varies in a narrow range $En_{0.38\text{-}0.39}$ $Fs_{0.15}$ $Wo_{0.47}$.

3.3.3 Feldspars

Plagioclase shows various chemical compositions from albite to bytownite in the amphibolites (Fig. 11).

In the D31 sample of *Group1*, the textural relations or core to rim zoning of the plagioclases was not well distinguished due to the limitations of the "original surface" method. Its composition varies from oligoclase to andesine with $An_{23.0\text{-}30.0}$. In the D05 and D13 stone axes, a labradorite composition with a narrow range of $An_{54.3\text{-}61.9}$ is present in the core (Pl1), presumably as a relict magmatic phase, while at the rim (Pl2) it is andesine with $An_{47.1\text{-}49.9}$ (Table 3). In the D12, D30 and D33 stone implements, albite ($An_{0.0\text{-}6.7}$) is the pre-kinematic plagioclase (Pl1) (Table 3). In samples D30 and D33, oligoclase ($An_{15.9\text{-}29.6}$) (Fig. 11), and in the D12 sample andesine ($An_{37.9\text{-}44.5}$) are the post-kinematic phases (Pl2) (Table 3).

In samples D04, D08, D45 and D48 of *Group2*, it was not possible to define the textural relations of plagioclases with andesine ($An_{40.3\text{-}49.5}$) and labradorite ($An_{50.9\text{-}64.8}$) compositions. In the stone implements C02 and D15, plagioclase of labradorite and bytownite composition ($An_{63.1\text{-}89.0}$) is a relict phase (Pl1) while oligoclase-andesine ($An_{13.4\text{-}46.5}$) is the typical composition for the rim (Pl2). For the other samples of *Group2*, the relict phases have values of $An_{24.4\text{-}65.7}$ for Pl1 and the post-kinematic minerals were albite, described with $An_{0.0\text{-}9.1}$ content as Pl2 (Table 3, Figs. 6—E, G, I). Potassic feldspar, as a relict phase is detected in *Group2b* (Figs. 6—E, G).

3.3.4 Other minerals

Epidote/clinozoisite is present in 9 samples (Table 6). Epidote/clinozoisite is mainly zoned, where Fe-content increases from the core to rim. In the D02 and D04 tools the amount of epidote and clinozoisite reaches 30 vol% (Fig. 7—B). *Biotite* was identified in tools C02, D15, and D17 (*Group2*). In samples C02 and D17, biotite is partially replaced by chlorite. Biotite occurs up to 50 μm in diameter. Its chemical compositions are listed in Table 7. *Ilmenite* forms idioblastic and hypidioblastic grains. In the samples B12 (Fig. 6—I), D15 and D18 (Fig. 6—C) ilmenite is partly replaced by titanite and contains magnetite and Ti-bearing magnetite as inclusions. MnO content in ilmenite from samples B12, D05 and D18 reaches 3.00-3.97 wt%. In sample D18 the size of ilmenite tablets reaches 600 μm in diameter. *Titanite* is a common accessory mineral and was found in nearly all the tools except B05, D13, D31 and D33. Its Al_2O_3 content is

typically high, varying in the range of 1.26-5.79 wt%. The highest value was recorded in the D05 sample but shows elevated values (2.28-4.01 wt%) in the B04, D15, D18 and D45 samples as well.

Magnetite is observed in the D04, D18, D21 and D33 samples. In D04 it is distributed along foliations with grain size up to 200 µm (Fig. 7—B). In tool D18, magnetite and Ti-bearing magnetite (TiO_2: 4.29 wt%) is recognized as inclusions in Mn-bearing ilmenite (Fig. 6—C). *Chlorite* was observed in five samples. In sample D13, chlorite of clinochlore composition is present at the contact of actinolite and epidote. In tool D02 it was observed at the rim of magnesio-hornblende. In sample D04, chlorite developed inside hematite and both in D02 and D04 samples chlorite was identified as chamosite. The chemical compositions of the chlorites are presented in Table 8.

4. Discussion

4.1 Thermobarometric estimations

As no garnet was found in the studied samples, the application of thermobarometric methods was limited. Since amphibole is a common mineral present in all amphibolite polished stone tools, the single Ca-amphibole approach of Gerya et al. (1997) was applied to calculate peak pressure and temperature ($P_{(Tmax)}$-T_{max}) conditions. The method was modified for Fe^{3+} by Zenk & Schulz (2004). Based on their suggestion, the 13CNK method (Locock, 2014) was used to determine the amphibole formulae. In this method, the absolute errors of the calculation are generally reduced to ±1.2 kbar and ±37 °C.

Group1

In sample D33, the magnesio-hornblende in the rim implies T_{max} 460 °C and $P_{(Tmax)}$ 2.8 kbar. In the D05 sample, tschermakite which rims magnesio-hornblende crystallized at 540 °C and 5.3 kbar. The D12 and D13 samples have very similar mineral assemblages and their P-T data calculated from magnesio-hornblende in the rim yield T_{max} of 560–570 °C and $P_{(Tmax)}$ of 5 kbar. Tschermakite in the rim (Table 3) in D30 and D31 samples implies T_{max} 615–635 °C and 5–6 kbar for $P_{(Tmax)}$. In D30, pargasite which rims magnesio-hornblende yielded T_{max} of 615 °C and 5.6 kbar for $P_{(Tmax)}$ (Table 9). In the D31 sample, the pargasite rim (Table 3) crystallized at 635 °C and 6.2 kbar and the magnesio-hornblende core (Table 3) yields the same P-T data (Table 9, Fig. 12).

Group2

In sample D08 of *Group2a*, tschermakite occuring along with magnesio-hornblende yielded 600 °C and 4.8 kbar in Table 9. In sample B12, the core pargasite recorded 670 °C and 6.5 kbar, the core sadanagaite yields similar data of 680 °C and 7.3 kbar. In the D47 sample, core pargasite crystallization recorded 690 °C and 7.0 kbar. In the D48 sample (*Group2b*), ferro-pargasite crystallization yielded T_{max}: 590 °C and $P_{(Tmax)}$ 4.6 kbar. In sample D17 of *Group2d*, ferro-pargasite rimmed by actinolite reached 610

°C and 5.7 kbar. In the other samples *of Group2*, the peak metamorphism was determined from magnesio-hornblende with T_{max} of 450–610 °C and $P_{(Tmax)}$ of 2.8–5.7 kbar (Table 9).

Plotting the T_{max} versus the $P_{(Tmax)}$ values, a continuous transition of simultaneously increasing values in the medium-temperature- and high-temperature fields can be observed (Table 9, Fig. 12). The medium-temperature group presents T_{max} ≈550 °C and $P_{(Tmax)}$ ≈5.3 kbar. For the high-temperature group, in which tschermakite-, pargasite-bearing amphibolite implements are present, the thermal maximum, T_{max} ≈600 °C and $P_{(Tmax)}$ 5–6 kbar are characteristic. The sadanagaite-bearing sample (B12) and a pargasite-bearing sample (D47) reached the highest peak temperatures. The B12 sample suggests T_{max} of 680 °C and $P_{(Tmax)}$ of 7.3 kbar and the D47 sample yields T_{max} of 690 °C and $P_{(Tmax)}$ of 7.0 kbar (Table 9, Fig. 12).

The tools in *Group2* were overprinted by greenschist facies metamorphism as magnesio-hornblende and actinolite surrounding earlier crystallized Ca-amphiboles.

The results of the thermobarometric calculations are listed in Table 9 and plotted in Fig. 12.

Based on the mineral assemblage and textural relationships, two metamorphic events can be recognized in both groups. In *Group1*, the M1 event is featured by the greenschist-amphibolite facies assemblage involving zoned Ca-amphibole with lower Al(tot). The M2 event is represented by higher Al(tot) values, indicating a progressive increase of pressure and temperature from the greenschist-amphibolite boundary to the amphibolite facies. In *Group2* the amphibolite facies M1 event was followed by the M2 event which was a retrograde stage of greenschist metamorphism recorded by the appearance of actinolite rimmed magnesio-hornblende, tschermakite, pargasite or sadanagaite and by the formation of albite, chlorite, epidote and titanite.

4.2. Possible provenance fields

Our petrological and mineralogical data were compared to the amphibolite bodies of Gemericum, Veporicum, Tatricum and Zemplinicum in Slovakia (Fig. 2) (Král' et al.,1997). Since amphibolite is a common and abundant raw material, the largest and the nearest amphibolite bodies are assumed to be the material sources for the investigated amphibolite stone implements. According to Přichystal (2013), stone raw material of polished implements could also have originated from riverbeds, furthermore Török (1996) declares that amphibolite is one of the most common pebble in Slaná- and Hornád-riverbeds; so the major rivers of Slovakia are also plotted on the map (Fig. 2).

The bulk chemistries of Gemericum, Veporicum and Tatricum amphibolites are very similar to each other and also to that of our samples, having subalkaline, tholeiitic character (Fig. 3) (Bajanik & Hovorka, 1981, Hovorka et al., 1993, Ivan et al., 2001, Faryad et al., 2005, Ivan & Méres, 2015). On the AFM diagram, the distribution of the data of the samples and the data of the possible provenance fields overlap each other (Fig. 4) (Bajanik & Hovorka, 1981, Hovorka et al., 1993, Ivan et al., 2001, Faryad et al., 2005, Ivan & Méres, 2015). Using only the major element composition of bulk chemistry, the provenance

field cannot be specified. Magnesio-hornblende and actinolite are very common minerals in amphibolites. Based only on their presence, selecting the provenance field is nearly impossible. Regarding the fact that systematic archaeometrical work on amphibolite implements has not been done which we could compare to, we have used various diagnostic minerals as well as the typical thermobarometric P-T data of the amphiboles for comparison to the data of the possible source regions.

All the above lithotectonic units where amphibolite occurs show multiphase (Variscan and Alpine) metamorphic evolutions with various intensities. Some localities do not show traces of the Alpine overprint at all, while others did not preserve relict textures of the Variscan metamorphic event (Bezák et al., 1993, Hovorka et al., 1993). Prograde textured amphibolites were preserved in some outcrops in the Ochtiná group (Novotná et al., 2015) and some places in the Veporicum and Tatricum (Krist et al., 1992). Most of the amphibolite occurrences show a retrograde overprint as well. The two subsequent metamorphic events can be characterized by significantly different metamorphic gradients. For the Variscan event 40 °C/km is typical, while the Alpine event suggests 10 °C/km (Bezák et al., 1993). The results of the thermobarometric calculations (according to Gerya et al., 1997, Zenk and Schulz 2004) (Fig. 12) show that all the studied samples fit well to the Variscan metamorphic gradient (Bezák et al., 1993); no trace of a high pressure, low-medium temperature overprint is observable. The Variscan metamorphic gradient (Bezák et al., 1993) (Fig. 12) and the Variscan P-T loop (Putiš et al., 1997) (Fig. 13) cover all the available fields that are considered here as possible source regions for the present group of amphibolite polished implements. The thermobarometric data of some possible provenance fields and the samples fit each other well as shown in Fig. 13. Regarding Tatricum, the Little Carpathians can be considered as a possible source region, while the thermobarometric data of Tribeč Mountains exclude these fields as source regions (Fig. 13).

In *Group1* the tschermakite- and pargasite-bearing prograde textured samples reached the highest metamorphic grade. In *Group1* the estimated thermobarometric data mostly range 540-635 °C and 5-6.2 kbar. But the D33 sample has a lower T_{max} 460 °C and $P_{(Tmax)}$ 2.8 kbar. Comparing to the prograde textured amphibolites from the Ochtiná group (Novotná et al., 2015) and sporadically from Veporicum and Tatricum (Krist et al., 1992) the majority of these *Group1* samples very likely originated from one of these areas (Table 10). According to the P-T estimation of D30 and D31, they correlate obviously to GAC-Klátov. D05, D12, D13 samples fit well to the Ochtiná group, but the P-T data of the Branisko, Čierna Hora, Čierny Balog, Little Carpathians and GAC-Klátov territories also match well. The D33 implement can be originated not only from Ochtiná group but Čierna Hora too (Fig. 13) (Table 10).

In the B12 sample (*Group2a*), besides the ordinary amphiboles, the uncommon sadanagaite and ferro-sadanagaite, as well as pargasite and ferro-pargasite also appear. The compositional range of these rare amhiboles is equivalent to pargasite and tschermakite, respectively, according to the previous nomenclature of amphiboles (Leake et al., 1997). Tschermakite, pargasite and their ferroan counterparts

were found in several samples: D05, D30, D31 (*Group1*), B12, D08, D47 (*Group2a*), D45 (*Group2c*), D48 (*Group2b*), D17 (*Group2d*). These samples have reached the highest metamorphic temperature (Fig. 12, Table 9). Results on pargasite-bearing Variscan amphibolites were published by Radvanec et al. (2017) in the GAC (Gneiss-Amphibolite Complex), Klátov area. Tschermakite-bearing amphibolites occur in several localities: the Ochtiná group (Novotná et al., 2015), Čierny Balog (Putiš et al. 1997), Čierna Hora (Faryad & Jacko, 2002) and also the Little Carpathians (Ivan et al., 2001). The calculated thermobarometric data of B12 and D47 samples would agree with the material originated from Zemplinicum or GAC-Klátov regions. The estimated P-T data and the mineral assemblage of D17 and D48 pargasite-bearing implements fit well to GAC-Klátov, but the Ochtiná group, Branisko Mountains and even the distant Little Carpathians cannot be excluded. The D08 (*Group2*) sample matches well to the Ochtiná group, Branisko or the Little Carpathians, but Stražovské Mountains can be considered also (Fig. 13) (Table 10).

Two epidote-rich amphibolite implements, D02 and D04 samples (*Group2a*) can be originated from Ochtiná group or GAC-Klátov. The calculated T_{max} ≈500 °C and $P_{(Tmax)}$ ≈3.7 kbar are similar for the two stone implements (Fig. 13).

The D18, D21 and D32 samples from *Group2a*, have a very common amphibolite mineral assemblage without any diagnostic minerals and their estimated P-T data overlap with earlier published thermobarometric data of numerous possible provenance fields: Branisko Mountains, Čierna Hora, Octhiná group, GAC-Klátov or even with the Little Carpathians. (Fig. 13).

Potassic feldspar is present as a relict phase in *Group2b*. Hence this variety may be correlated to Čierna Hora and Branisko Mountains (Faryad & Jacko, 2002) amphibolites as these rocks contain potassic feldspar and Mn-bearing ilmenite as accessory phases. Furthermore, plagioclase with a maximum An_{43} content was mentioned from here. The C02 sample contains bytownite as a relict phase also. The plagioclase compositions of these three stone tools and their mineral assemblages are rather similar to the amphibolites of Čierna Hora. Amphibolites from Čierna Hora have a tholeiitic basalt and basaltic andesite composition (Faryad et al., 2005), similar to the above mentioned three implements. The well-matching thermobarometry data of *Group2b* and Čierna Hora confirm the correlation (Figs. 6—G, E, 14). In the case of the D48 sample the estimated P-T values indicate Branisko Mountain as a possible provenance field, but the Ochtiná group and GAC-Klátov cannot be excluded either (Table 10).

Group2c corresponds to clinopyroxene- and biotite-bearing amphibolites described from Gemericum (Faryad, 1997, Hovorka & Spišiak, 1997). The mineral assemblage and the estimated thermobarometry data of *Group2c* indicate GAC-Klátov as a possible provenance field, but Branisko Mountain, Čierna Hora and Little Carpathians cannot be excluded because of the matching P-T data. Biotite-bearing amphibolites were earlier investigated from the above-mentioned territories (Vozárová & Faryad, 1997, Ivan et al., 2001) (Fig. 13).

Higher magnetic susceptibility values were measured from some samples of *Group1* (D33) and *Group2* (B12, C02, D04, D08, D18), although the presence of magnetite was not always supported by the EDS/SEM observations. Greenstones and amphibolites with high magnetite content were described from the Little Carpathians (Ivan et al., 2001) and the Slovak Ore Mountains (Faryad & Peterec, 1987). Therefore, the raw material of these polished stone tools might originate from these territories (Table 10).

The schematic map of amphibolite outcrops and the major rivers shows that the Hornád- and Slaná rivers cross the Gemericum, Veporicum and Zemplinicum regions and flow to Borsod-Abaúj-Zemplén county, the archaeological collecting territory of the investigated amphibolite implements (Fig. 2). This confirms these rivers as deliverers of raw materials from the source areas.

Conclusions

Based on the mineralogical assemblages and textural relations of the amphibolite stone implements, two groups have been distinguished: *Group1* and *Group2*. Six samples preserving the features of prograde metamorphism were assigned to *Group1*. *Group2* contains most of the samples which are overprinted by retrograde metamorphism. The results of thermobarometric calculations of the investigated polished stone tools were compared to the earlier published thermobarometric data for the amphibolite field samples, as expressed in the Variscan metamorphic gradient (Fig. 12) and in Variscan P-T loop (Fig. 13).

Metamorphic evolution, thermobarometric data, petrographic-, and mineralogical observations have been taken into account in the classification of the possible provenance fields of the amphibolite polished stone implements. Even the distance of the source area and the archaeological localities is not a negligible factor because amphibolite is a diverse, common and a widespread rock in Slovakia. According to this fact, we suppose that the nearby amphibolite outcrops may be considered particularly (Table 10) For the *Group1* and for the D02, D04 samples of *Group2a* Ochtina group and GAC Klátov is the most likely provenance fields, but for the *Group1* Veporicum and Tatricum cannot be excluded either. In the case of D04 Little Carpathians is a presumptive area. The B12 and D47 samples (*Group2a*) have reached the highest metamorphic grade, they may originate from GAC-Klátov or the Zemplinicum unit. D08, D18, D21 and D32 samples of *Group2a* may have derived from several fields of Gemericum, Veporicum, Tatricum. The most possibble source areas of the Group2b are Čierna Hora and Branisko, but in the case of C02 sample Tatricum cannot be excluded either, furthermore the D48 implement can be originated from GAC-Klátov or Ochtina group too. The samples of Group2c and Group2d most likely stem from GAC Klátov, but the possible provenance field of Group2c may be Branisko, Čierna Hora or the LIttle Carpathians as well (Table 10).

To identify the provenance field at site level in the case of amphibolite archaeological findings, cannot be solved without specific minerals or signs except for individual cases. However, because of the overlap of the P-T values of the provenance fields and the uncertainty of the estimated P-T values for the archaeological samples, it is not possible to unambiguously assign any provenance field to any single sample. Based on the mineral assemblages, textural features and thermobarometry estimations it can be concluded that the provenance fields of our samples could be the Gemericum, Veporicum, Tatricum and the Zemplinicum (Figs. 13, 14) (Table 10).

As amphibolite is a widespread and common rock in Slovakia no correlation has been detected between lithotypes and the typology of the artefacts, furthermore nor in their chronological and cultural aspects.

Acknowledgements

This research was partly funded by the Hungarian Scientific Research Fund (OTKA), under the contracts Nos. K100385. and K131814. The authors would like to express their thanks to Professor Shah Wali Faryad for very helpful discussions during preparation of the manuscript and for clarifying the metamorphic history of the possible provenance fields. The authors also thank Jesse L. Weil for careful reading and correcting the manuscript text.

References

Bajaník S., Hovorka D. 1981: The amphibolite facies metabasites of the Rakovec group of Gemericum (The Western Carpathians). Geologica Carpathica 32, 679-705.

Bendő Zs., Oláh I., Péterdi B., Szakmány Gy., Horváth E. 2013: Non-destructive SEM-EDX analytical method for polished stone tools and gems: opportunities and limitations. Archeometriai Műhely 10/1, 51-66.

Bezák V., Sassi F. P., Spišiak J, Vozárová A. 1993: An outline of the metamorphic events recorded in the Western Carpathians (Slovakia). Geologica Carpathica 44, 351-364.

Bradák B., Szakmány Gy., Józsa S., Přichystal A. 2009: Application of magnetic susceptibility on polished stone tools from Western Hungary and the Eastern part of Czech Republic (Central Europe). Journal of Archaeological Science 36, 2437-2444. http://dx.doi.org/10.1016/j.jas.2009.07.001.

Csengeri P. 2011: Middle Neolithic face vessels from Garadna (Hornád valley). Herman Ottó Múzeum Évkönyve 50., 67-104. (in Hungarian).

Csengeri P. 2013: Later groups of Alföld Linear Pottery in Northeast of Hungary. (Recent research from Borsod-Abaúj-Zemplén county). Eötvös Lorán University PhD thesis. pp. 311. (in Hungarian).

Csengeri P. 2015: Middle Neolithic painted pottery from Borsod-Abaúj-Zemplén county, North-Eastern Hungary, in: Virág C. (Ed.): Neolithic cultural phenomena in the upper Tisza basin international conference, Satu Mare, pp. 127-160.

Dyda M. 1997: Disturbance of the Variscan metamorphic complex indicated by mineral reactions, P-T data and crystal size of garnets (Malé Karpaty Mts.), in: Grecula P., Hovorka D., Putiš M. (Eds.), Geological evolution of Western Carpathians., Bratislava, pp. 333-342.

Faryad S. W. 1990: Gneiss-amphibolite Complex of the Gemericum. Mineralia Slovaca 22, 303-318.

Faryad S. W. 1995: Geothermobarometry of metamorphic rocks from the Zemplinicum (Western Carpathians, Slovakia). Geologica Carpathica 46, 113-123.

Faryad S. W. 1997: Metamorphic petrology of the Early Paleozoic low-grade rocks in the Gemericum, in: Grecula P., Hovorka D., Putiš M. (Eds.), Geological evolution of Western Carpathians., Bratislava, pp. 309-314.

Faryad S. W. 1999: Metamorphic evolution of the eastern part of the Western Carpathians, with emphasis on Meliata Unit. Acta Montanistica Slovaca 4 (2) 148-169.

Faryad S. W., Jacko S. 2002: New data on P-T conditions of Variscan and Alpine metamorphism from the Čierna Hora Mts., Veporic Unit, Western Carpathians (Slovakia). Geologica Carpathica 53, Special issue (CD). Proceedings of XVII. Congress of Carpathian-Balkan Geological Association Bratislava, September 1-4, 2002.

Faryad S. W., Peterec D. 1987: Manifestations of skarn mineralization in the eastern part of the Spišsko-Gemerské Rudohorie Mts. Geologica Carpathica 38, 111-128.

Faryad S. W., Spišiak J. 1999: Klátov-Early Paleozoic amphibolite facies rocks. Acta Montanistica Slovaca 4 (2) pp. 173.

Faryad S. W., Vozárová A. 1997: Geology and metamorphism of the Zemplinicum basement unit (Western Carpathians), in: Grecula P., Hovorka D., Putiš M. (Eds.), Geological evolution of Western Carpathians., Bratislava, pp. 351-358.

Faryad S. W., Vozárová A., Jacko S. 1999: Branisko – amphibolites and gneisses of Tatric and Veporic basement. Acta Montanistica Slovaca 4, 182.

Faryad S. W., Ivan P., Jacko S. 2005: Metamorphic petrology of metabasites from the Branisko and Čierna Hora Mountains (Western Carpathians, Slovakia). Geologica Carpathica 56, 3-16.

Gerya T. V., Perchuk L. L., Triboulet C., Audren C., Sez'ko A. I. 1997: Petrology of the Tumanshet Zonal Metamorphic Complex, Eastern Sayan. Petrology 5, 503-532.

Hawthorne F. C., Oberti R., Harlow G. E., Maresch W. V., Martin R. F., Schumacher J. C., Welch M. D. 2012: IMA report: Nomenclature of the amphibole supergroup. American Mineralogist 97, 2031-2048.

Hovorka D., Cheben I. 1997: Raw materials of the Neolithic polished stone artefacts from the site Bajč. Mineralia Slovaca 29, 210-217. http://dx.doi.org/10.2138/am.2012.4276.

Hovorka D, Spišiak J. 1997: Medium-grade metamorphics of the Gemeric unit (central Western Carpathians). in: Grecula P., Hovorka D., Putiš M. (Eds.), Geological evolution of Western Carpathians, Bratislava, pp. 315-332.

Hovorka D., Méres S., Ivan P. 1993: Pre-Alpine Western Carpathians basement complexes: Lithology and geodynamic setting. Mitt. Österr. Geol. Ges., 86, 33-44.

Hovorka D., Illášová L., Pavúk J. 2001: Raw materials of Aeneolithic stone polished artifacts found on type locality of the Lengyel culture: Svodín, Slovakia. Mineralia Slovaca 33, 343-350.

Irvine T. N., Baragar W. R. A. 1971: A guide to the chemical classification of the common volcanic rocks. Canadian Journal of Earth Sciences 8, 523-548.

Ivan P., Méres S. 2015: Geochemistry of amphibolites and related graphitic gneisses from the Suchý and Malá Magura Mountains (central Western Carpathians) – evidence for relics of the Variscan ophiolite complex. Geologica Carpathica 66, 347-360. https://doi.org/10.1515/geoca-2015-0030.

Ivan P., Méres Š., Putiš M. Kohút M. 2001: Early Paleozoic metabasalts and metasedimentary rocks from the Malé Karpaty Mts. (Western Carpathians): Evidence for rift basin and ancient oceanic crust. Geologica Carpathica 52, 67-78.

Janák M., Hovorka D., Hurai V., Lupták B., Méres Š., Pitoňák P., Spišiak J. 1997: High-pressure relics in the metabasites of the Western Carpathians pre-alpine basement. in: Grecula P., Hovorka D., Putiš M. (Eds.), Geological evolution of Western Carpathians, Bratislava, pp. 301-38.

Kalicz N. & Makkai J. 1977: Die Linienbandkeramik in der Groβen Ungarischen Tiefebene, Akadémiai Kiadó, Budapest, pp. 386.

Kasztovszky Zs., T. Biró K., Markó A., Dobosi V. 2008: Cold neutron prompt gamma activation analysis – a non-destructive method for characterization of high silica content chipped stone tools and raw materials. Archaeometry 50, 12-19. http://dx.doi.org/10.1111/j.1475-4754.2007.00348.x.

Kereskényi E., Kristály F., T. Biró K., Péterdi B., Bendő Zs., Rózsa P. 2015a: The first results of a new project: archaeometrical investigation of Neolithic polished stone tools of Herman Ottó Museum. *Acta Mineralogica-Petrographica Abstract Series* 9, 30.

Kereskényi E., Kristály F., Fehér B., Rózsa P. 2015b: The first results of the Neolithic polished stone tools of Herman Ottó Museum. From magma genesis to regional lithosphere-forming processes. 6th Petrological and geochemical Meeting. *University of Szeged, Department of Mineralogy, Geochemistry and Petrology,* 71-74. (in Hungarian).

Kereskényi E., Szakmány Gy., Fehér B., Kasztovszky Zs., Kristály F., Rózsa P. 2018: New archaeometrical results related to Neolithic blueschist stone tools from Borsod-Abaúj-Zemplén County, Hungary. Journal of Archaeological Science: Reports 17, 581-596.

Kráľ J., Hess J. C., Kober B., Lippolt H. J. 1997: $^{207}Pb/^{206}Pb$ and $^{40}Ar/^{39}Ar$ age data from plutonic rocks of the Strážovské vrchy Mts. basement, Western Carpathians, in: Grecula P., Hovorka D., Putiš M. (Eds.), Geological evolution of Western Carpathians, Bratislava, pp. 253-260.

Krist E., Korikovskij P. S., Putiš M., Janák M., Faryad S. W. 1992: Geology and petrology of metamorphic rocks of the Western Carpathians crystalline complexes, Comenius University, Bratislava, pp. 7.

Leake B. E., Wooley A. R., Arps C. E. S., Birch W. D., Gilbert M. C., Grice J. D., Hawthorne F. C., Kato A., Kisch H. J., Krivovichec V. G., Linthout K., Laird J., Mandarino J. A., Maresch W. V., Nickel E. H., Rock N. M. S., Schumacher J. C., Smith D. C., Stephenson N. C. N., Ungaretti L., Whittaker E. J. W., Youzhi G. 1997: Nomenclature of amphiboles: report of the Subcommittee on Amphiboles of the International Mineralogical Association, Commission on New Minerals and Mineral Names. The Canadian Mineralogist 35, 219-246.

Locock, A. 2014: An excel spreadsheet to classify chemical analyses of amphiboles following the IMA 2012 recommendations. Computers & sciences 62, 1-11. http://dx.doi. org/10.1016/j.cageo.2013.09.011.

Méres S., Hovorka D., Cheben I. 2001: Provenience of polished stone artefacts raw materials from the site Bajč-Medzi kanálmi (Neolithic, Slovakia). Slovak Geological Magazin 7, 369-381.

Morimoto N. 1989: Nomenclature of pyroxenes. Canadian Mineralogist 27, 143-156.

Novotná N., Jeřábek P., Pitra P., Lexa O., Racek M. 2015: Repeated slip along a major decoupling horizon between crustal-scale nappes of the Central Western Carpathians documented in the Ochtiná tectonic mélange. Tectonophysics 646, 50-64.

Plašienka D., Grecula P., Putiš M., Kovač M., Hovorka D. 1997: Evolution and structure of the Western Carpathians: an overview. in: Grecula P., Hovorka D., Putiš M. (Eds.), Geological evolution of Western Carpathians, Bratislava, pp. 1-24.

Putiš M., Filová S., Korikovsky S. P., Kotov A. B. 1997: Layered metaigneous complex of the Veporic basement with features of the Variscan and Alpine thrust tectonics (the Western Carpathians), in: Grecula P., Hovorka D., Putiš M. (Eds.), Geological evolution of Western Carpathians, Bratislava, pp. 175-196.

Přichystal A. 2013: Lithic raw materials in prehistoric times of Eastern Central Europe. Masaryk University, Brno. pp. 200.

Radvanec M., Németh Z., Král J., Pramuka S. 2017: Variscan dismembered ophiolite suite fragments of Paleo-Tethys in Gemeric unit, Western Carpathians. Mineralia Slovaca 49, 1-48.

Révay Zs. 2009: Determining elemental composition using prompt gamma activation analysis. Analytical Chemistry 81, 6851-6859. http://dx.doi.org/10.1021/ac9011705.

Selján É. 2005: The Tiszai cultured Szerencs-Taktaföldvár in the late Neolithicum. Diploma thesis, Eötvös Loránd University, Budapest. (in Hungarian).

Szakmány Gy., Kasztovszky Zs. 2004: Prompt Gamma Activation Analysis, a new method in the archaeological study of polished stone tools and their raw materials. European Journal of Mineralogy 16, 285-295. http://dx.doi.org/10.1127/0935-1221/2004/0016-0285.

Szakmány Gy., Kasztovszky Zs., Szilágyi V., Starnini E., Friedel O., T. Biró K. 2011a: Discrimination of prehistoric polished stone tools from Hungary with non-destructive chemical Prompt Gamma Activation Analyses (PGAA). European Journal of Mineralogy 23, 883-893. http://dx.doi.org/10.1127/0935-1221/2011/0023-2148.

Szakmány Gy., Starnini E., Horváth F., Bradák B. 2011b: Investigating trade and exchange patterns in prehistory: Preliminary results of the archaeometric analyses of stone artefacts from Tell Gorzsa (South-East Hungary), in: Turbanti-Memmi, I., (Eds.): Proceedings of the 37th International Symposium on Archaeometry, 12th-16th May 2008, Siena, Italy, *Springer*, Berlin Heidelberg, pp. 311-319.

Szentmiklósi L., Belgya T., Révay Zs., Kis Z. 2010: Upgrade of the prompt gamma activation analysis and the neutron-induced prompt gamma spectroscopy facilities at the Budapest Research Reactor. Journal of Radioanalytical and Nuclear Chemistry 286, 501–505. http://dx.doi.org/10.1007/s10967-010-0765-4.

Török E. (1996): Hazai kavicsmezők anyagának szilárdsága a halmazjellemzők tükrében. (The strength of the Hungarian gravel fields according to set parameters.) Földtani Közlöny 126/1, pp. 117-129 (in Hungarian).

Vozárová A., Faryad S., W. 1997: Petrology of Branisko crystalline rock complex in: Grecula P., Hovorka D., Putiš M. (Eds.), Geological evolution of Western Carpathians, Bratislava, pp. 343-350.

Zenk M., Schulz B. 2004: Zoned Ca-amphiboles and related P-T evolution in metabasites from the classical Barrovian metamorphic zones in Scotland. Mineralogical Magazine 68, 769-786.

Fig. 1: Schematic map showing archaeological localities of amphibolite stone tools that are deposited at the Herman Ottó Museum. Abbreviation: *BAZ*: Borsod-Abaúj-Zemplén.

Fig. 2: Geographical setting of the main lithotectonic units containing amphibolite bodies of the Central-Western Carpathians and depicting the principal rivers of Slovakia. The schematic map is modified after Král' et al. (1997). Abbreviations on the map: B & CH: Branisko and Čierna Hora Mountains, G: Gemericum, V: Veporicum, LT: Low Tatras, HT: High Tatras, LF: Low Fatras, HF: High Fatras, S: Strážovské Mountains, Z: Žiar Mountains, I: Inovec Mountains, T: Tribeč Mountains, LC: Little Carpathians.

Fig. 3: Amphibolite implements from the Herman Ottó Museum and their potential provenances plotted in the Total Alkali- Silica (TAS) diagram.

Fig. 4: AFM diagram of the investigated amphibolite implements and their possible fields of amphibolite localities plotted in AFM (Irvine and Baragar, 1971) diagram. A = alkali (Na_2O+K_2O), F = FeO (total), M = MgO. IAT = island arc tholeiite, MORB = mid-ocean ridge basalt.

Fig. 5: A—B Macroscopic and BSE images of the coarse-grained sample D12 (*Group1a*). C—D Macroscopic and BSE images of the coarse-grained sample D13 (*Group1a*). E—F Macroscopic and BSE images of sample D30 (analysed by original surface) (*Group1b*).

Fig. 6: A—B Macroscopic and BSE images of the coarse-grained, ilmenite-rich sample D18 (*Group2a*). C—Ilmenite is partly replaced by titanite with magnetite inclusions in the BSE image of the sample D18. D—E Macroscopic and BSE images of the sample B04 (*Group2b*). F—G Macroscopic and BSE images of the sample B05 (*Group2b*). H—I Macroscopic and BSE images of the sample B12 (*Group2a*).

Fig. 7: A—B Macroscopic and BSE images of the foliated, epidote-rich D04 sample (*Group2a*). C—D Macroscopic and BSE images of the well-foliated D08 sample (*Group2a*).

Fig. 8: Chemical composition of calcic amphiboles of *Group1* amphibolites plotted in the $^{C}(Al+Fe^{3+}+2Ti)$ vs. $^{A}(Na+K+2Ca)$ diagram. Arrows indicate the phase changes from core to rim.

Fig. 9: Chemical composition of calcic amphiboles of *Group2* and their potential provenances plotted in the $^{C}(Al+Fe^{3+}+2Ti)$ vs. $^{A}(Na+K+2Ca)$ diagram. The arrows indicate the phase changes from core to rim. Circles signify the samples analysed by the "surface method".

Fig. 10: Clinopyroxene compositions of D15, D34, D45 samples plotted in the En-Fs-Wo ternary diagram (Morimoto, 1989).

Fig. 11: Compositions of feldspars plotted in Or-Ab-An ternary diagram

Fig. 12: P-T diagram showing thermobarometric estimated calculation results T_{max} and $P(_{Tmax})$ of the amphibolite polished stone tools plotted with the Variscan (V) and Alpine (A) metamorphic gradient (Bezák et al., 1993). Red coloured symbols signify the *Group1* samples, while the other samples are in *Group2.*

Fig. 13: Thermobarometric data of amphibolite implements and of field samples from Gemericum, Veporicum, Tatricum and Zemplinicum. The grey loop indicates the estimated Variscan P-T loop (Putiš et al., 1997). Red coloured symbols signify the *Group1* samples, while the other samples are all in *Group2*. Abbreviations: GAC-K: Gneiss Amphibolite Complex, Klátov; C-L: Čierna Hora, lower unit; B: Branisko Mountains; CB: Čieny Balog; Ze: Zemplinicum; T: Tribeč Mountains; Sv: Stražovské Mountains; LC: Little Carpathians.

Fig. 14: The schematic geological setting of the amphibolites from the surrounding area after Král' et al., (1997). The arrows show the relation between the possible provenance fields and archaeological localities of the studied stone implements. For the abbreviations on the map, see those on Fig. 13.

Table 1

Amphibolite implements from the collection of the Herman Ottó Museum giving the different analytical methods and magnetic susceptibility (MS) values in units of 10^{-3} Sl. (Y: yes; N: no; *: "Original surface", semi-quantitative method; AVK: Alföld Linear Pottery).

Sample	Inventory number	Locality	EDS/ SEM	PGAA	MS	Archaeological typology	Age	Culture / Phase
B04	70.1.23	Szerencs-Taktaföldvár	Y	Y	0.73	Flat chisel	Late Neolithic	Tisza
B05	70.1.24	Szerencs-Taktaföldvár	Y	Y	0.63	Flat chisel	Late Neolithic	Tisza
B12	74.44.15	Szerencs-Taktaföldvár	Y	Y	6.47	Flat chisel	Late Neolithic	Tisza
C02	53.206.3	Tiszadorogma	Y	Y	10.51	Flat chisel	Middle Neolithic	AVK
D02	70.1.149	Szerencs-Taktaföldvár	Y	Y	0.52	Flat chisel	Late Neolithic	Tisza
D04	58.42.2	Fancsal-farm	Y	Y	46.8	Flat chisel	Neolithic	Stray find
D05	not inventoried	Lidl Hejőkürt 2mh. S2106 2005. 06. 14.	Y	Y	1.69	Flat chisel	Middle Neolithic	AVK
D08	53.238.5	Szirmabesenyő's vicinity	Y	Y	17.17	Flat chisel	Middle Neolithic	Bükk AB, AVK
D12	53.248.1	Unknown	Y	Y	n.a.	Flat chisel	Neolithic	Stray find
D13	53.250.1	Bereg county	Y	N	0.68	Flat chisel	Neolithic	Stray find
D15	53.208.1	Emőd, Vaskó-sheer	Y	Y	0.62	Flat axe	Neolithic	Stray find
D17	74.44.11	Szerencs-Taktaföldvár	Y	Y	0.39	Flat chisel	Late Neolithic	Tisza
D18	not inventoried	Miskolc Aldi2 S153 2009. 09. 11.	Y	Y	24.33	Flat chisel	Middle Neolithic	AVK, Bükk
D21	53.160.20	Borsod/Derékegyháza (Edelény)	Y	Y	8.52	Shoe-last axe	Middle Neolithic	Bükk AB, B-C
D26	74.44.10	Szerencs-Taktaföldvár	N	Y	0.50	Flat chisel	Late Neolithic	Tisza
D30*	53.160.11	Borsod/Derékegyháza (Edelény)	Y	Y	1.69	Flat chisel	Middle Neolithic	Bükk AB, B-C
D31*	53.160.31a	Borsod/Derékegyháza (Edelény)	Y	N	1.44	Flat chisel	Middle Neolithic	Bükk AB, B-C

D32*	53.160.31b	Borsod/Derékegyháza (Edelény)	Y	Y	0.31	Shoe-last axe	Middle Neolithic	Bükk AB, B-C

Table 1 continued

Sample	Inventory number	Locality	EDS/ SEM	PGAA	MS	Archaeological typology	Age	Culture/ Phase
D33*	53.160.150	Borsod/Derékegyháza (Edelény)	Y	Y	29.62	Flat chisel	Middle Neolithic	Bükk AB, B-C
D34*	53.229.1	Muhi, Bala Hill	Y	Y	n.a.	Flat chisel	Neolithic	Unknown
D35	70.1.206	Szerencs-Taktaföldvár	N	Y	0.38	Axe fragment	Late Neolithic	Tisza
D37	67.13.3	Tolcsva's vicinity	N	Y	0.72	Flat axe	Neolithic	Unknown
D38	67.12.1	Egerlövő	N	Y	0.49	Shaft drilled axe	Neolithic	Unknown
D39	67.13.2	Tolcsva's vicinity	N	Y	n.a.	Shoe-last axe	Neolithic	Stray find
D40	53.187.3b	Hangács, Ludas Balk	N	Y	1.79	Shaft drilled axe	Neolithic	Unknown
D41	77.44.14	Szerencs-Taktaföldvár	N	Y	n.a.	Flat chisel	Late Neolithic	Tisza
D45*	72.11.303	Tiszavalk, Kenderföldek	Y	N	0.85	Flat chisel	Middle Neolithic	AVK
D47*	75.25.20	Unknown	Y	N	0.61	Flat chisel	Neolithic	Stray find
D48*	53.206.2	Tiszadorogma	Y	N	0.56	Tongue-shaped axe	Middle Neolithic	AVK

Table 2

PGAA results. The major components are given in wt%, the trace elements are in ppm. The amount of oxides is calculated from the elemental concentration, based on the oxidation numbers. The number of digits indicates the uncertainties of concentration values. "<D.L." stands for "less than the Detection Limit".

Sample	B04	B05	B12	C02	D02	D04	D05	D08	D12	D15	D17	D18
SiO_2	54.18	50.39	47.77	47.85	47.00	49.00	50.00	50.00	50.00	47.00	59.00	52.00
TiO_2	0.46	2.28	2.29	2.63	1.61	1.53	1.92	1.48	3.70	1.29	1.07	1.70
Al_2O_3	13.58	16.11	14.36	15.04	13.00	13.50	15.50	13.60	13.00	15.00	17.80	13.90
Fe_2O_3*	10.07	12.53	12.71	13.13	11.70	12.40	9.60	12.30	13.20	10.70	5.40	11.20
MnO	0.21	0.17	0.18	0.24	0.23	0.21	0.23	0.26	0.18	0.28	0.10	0.17
MgO	5.76	5.47	7.06	4.95	7.40	3.50	6.30	7.90	5.60	7.80	3.00	6.90
CaO	7.48	4.74	8.30	9.32	13.10	11.80	10.90	12.10	9.80	14.90	7.20	8.80
Na_2O	4.12	4.70	3.52	3.50	1.30	1.30	2.27	1.53	2.50	0.73	2.97	3.15
K_2O	1.04	0.38	1.47	0.86	0.13	0.18	0.25	0.12	<D.L.	0.19	1.17	0.24
H_2O	1.59	3.16	2.22	2.27	1.69	1.72	1.59	1.62	1.21	1.63	2.24	1.30
SO_3	1.38	<D.L.	<D.L.	<D.L.	2.60	1.22	1.72	0.43	0.48	<D.L.	<D.L.	0.41
Total	99.90	99.92	99.89	99.76	99.76	96.36	100.28	101.34	99.67	99.52	99.95	99.77
B	10	1	2	1	6	3	4	3	2	12	20	3
Cl	407	305	689	798	196	200	220	290	23	270	105	180
Sc	<D.L.	39	<D.L.	65	53	40	101	51	<D.L.	29	23	12
V	134	234	185	409	480	310	670	340	390	170	160	230
Cr	<D.L.	<D.L.	<D.L.	506	<D.L.	<D.L.	<D.L.	<D.L.	<D.L.	<D.L.	<D.L.	<D.L.
Co	<D.L.	<D.L.	<D.L.	<D.L.	<D.L.	<D.L.	<D.L.	<D.L.	<D.L.	<D.L.	<D.L.	<D.L.
Nd	<D.L.	<D.L.	29	<D.L.	15	<D.L.	21	33	34	21	22	17
Sm	1	4	4	5	2	2	3	2	6	2	3	5
Gd	2	6	5	7	4	4	5	4	7	3	4	7

* Total Fe as Fe_2O_3.

Table 2 continued

Sample	D21	D26	D30	D32	D33	D34	D35	D37	D38	D39	D40	D41
SiO_2	47.00	53.00	50.00	49.00	52.80	48.00	46.55	56.22	50.00	52.00	47.00	51.00
TiO_2	1.71	1.41	2.06	1.78	2.19	1.32	1.39	1.08	0.82	1.10	2.50	2.12
Al_2O_3	13.60	13.20	15.11	14.80	13.64	13.80	15.78	18.11	15.60	11.20	12.90	15.30
Fe_2O_3*	11.40	8.50	11.10	10.20	11.75	11.10	11.85	5.96	9.70	12.50	12.60	10.90
MnO	0.19	0.28	0.17	0.19	0.20	0.20	0.22	0.14	0.10	0.34	0.39	0.19
MgO	7.30	7.20	7.60	6.50	5.90	7.40	8.94	3.39	6.60	7.10	6.20	4.20
CaO	10.30	11.40	7.40	12.70	7.77	14.70	9.96	8.79	12.40	13.00	11.20	9.20
Na_2O	1.63	2.80	4.30	1.87	3.76	1.78	2.84	3.04	2.20	0.81	2.05	3.90
K_2O	0.16	0.32	0.33	0.16	0.42	0.25	0.44	1.00	0.28	0.40	0.31	0.82
H_2O	1.59	1.30	1.68	1.67	0.97	1.66	1.94	2.24	1.89	1.49	2.21	2.30
SO_3	5.00	0.59	0.64	1.28	0.53	<D.L.	<D.L.	<D.L.	<D.L.	0.31	2.70	<D.L.
Total	99.88	101.89	100.38	100.15	99.93	100.21	99.93	99.97	99.59	100.25	100.06	99.93
B	4	4	3	3	4	6	5	23	6	4	7	2
Cl	200	201	42	250	190	0	<D.L.	90	510	570	290	690
Sc	47	33	<D.L.	65	<D.L.	<D.L.	46	34	19	9	44	21
V	410	250	360	490	268	360	336	<D.L.	250	310	430	270
Cr	<D.L.	<D.L.	<D.L.	<D.L.	<D.L.	<D.L.	<D.L.	<D.L.	<D.L.	<D.L.	<D.L.	<D.L.
Co	<D.L.	<D.L.	<D.L.	<D.L.	<D.L.	<D.L.	<D.L.	<D.L.	<D.L.	<D.L.	<D.L.	<D.L.
Nd	14	21	32	19	<D.L.	80	<D.L.	22	230	20	16	30
Sm	3	3	4	3	7	2	3	4	1	2	4	3
Gd	4	4	7	5	10	4	5	5	2	3	5	4

* Total Fe as Fe_2O_3.

Table 3 Main diagnostic minerals of *Groups- 1* and *2* of amphibolite stone implements.

Sample	**Amphibole**		**Plagioclase**		**Kfs**	**Bi**	**Ep/Czo**	**Cpx**
Group1	core	rim	Pl1 (core)	Pl2 (rim)				
D05	Act; Mg-hb	Mg-hb; Tsch	Lab	And				
D12	Act	Mg-hb	Ab	And				
D13	Act	Mg-hb	Lab	And				
D30	Mg-hb	Tsch; Prg	Ab	Olg				
D31	Act; Mg-hb	Tsch; Prg	And, Olg	And, Olg				
D33	Act	Mg-hb; Mg-f-hb	Ab	Olg			X	
Group2								
Group2a								
B12	Sdg; Fsdg; Prg; Fprg	Mg-hb; Act	And	Ab			X	
D02	Mg-hb; Fhb	Act; Fact	Lab, And, Olg	Ab			X	
D04	Mg-hb	Mg-hb	Lab, And	Lab, And			X	
D08	Mg-hb; Mg-f-hb; Fe2-ftsch; Fe3-Ts	Act	Lab, And	Lab, And			X	
D18	Mg-hb	Act	Lab, And, Olg	Ab				
D21	Mg-f-hb	Mg-f-hb	Byt, And	Ab				
D32	Mg-hb	Act	And, Olg	Ab				
D47	Mg-hb; Prg; Fprg	Act	And	Ab			X	
Group2b								
B04	Mg-hb	Act	And, Olg	Ab	X			
B05	Mg-hb	Act; Fact	Lab, And	Ab	X			
C02	Fhb, Mg-hb	Fhb, Act	Byt	And, Olg	X	X		
D48	Fprg, Mg-hb	Fprg, Mg-hb	And, Lab	And, Lab	X		X	
Group2c								
D15	Mg-hb	Act	Byt, Lab	And		X	X	X
D34	Mg-hb	Mg-hb; Act	And	Ab				X
D45	Fhb	Act	Lab; And	Lab; And				X
Group2d								
D17	Fprg; Mg-hb	Mg-hb; Act	And, Olg	Ab		X	X	

Table 4 Chemical composition of amphiboles (*Group 1*).

No.	1	2	3	4	5	6	7	8
Sample	D05-15	D30	D30	D31	D30	D30	D31	D31
SiO_2	47.83	45.05	45.71	44.21	44.32	44.45	43.47	43.48
TiO_2	0.16	0.35	0.30	0.26	0.30	0.40	0.45	0.50
Al_2O_3	15.60	15.68	15.09	16.54	13.94	13.45	16.53	14.88
MnO	0.23	0.00	0.00	0.11	0.05	0.00	0.10	0.19
FeO*	12.60	9.14	9.12	10.40	12.34	14.51	11.44	12.54
Fe_2O_3*	0.00	3.66	4.04	2.93	2.10	0.00	1.45	1.60
MgO	8.80	12.21	11.56	10.65	11.48	11.62	10.91	10.98
CaO	10.80	8.82	9.16	10.28	11.15	11.29	10.88	11.63
Na_2O	1.64	2.76	2.63	2.34	2.06	1.97	2.58	1.88
K_2O	0.32	0.28	0.34	0.25	0.24	0.29	0.17	0.31
H_2O**	2.05	2.04	2.04	2.03	2.00	2.01	2.03	2.01
Total	**100.00**	**100.00**	**100.00**	**100.00**	**100.00**	**100.00**	**100.00**	**100.00**
Cation numbers based on 23 oxygens.								
Si	6.85	6.45	6.55	6.38	6.46	6.48	6.30	6.36
Al	1.15	1.55	1.45	1.62	1.54	1.52	1.70	1.64
Σ*T*	**8.00**	**8.00**	**8.00**	**8.00**	**8.00**	**8.00**	**8.00**	**8.00**
Ti	0.02	0.04	0.03	0.03	0.03	0.04	0.05	0.06
Al	1.48	1.10	1.10	1.19	0.86	0.79	1.13	0.92
Fe^{3+}	0.00	0.40	0.44	0.32	0.23	0.23	0.16	0.18
Mn^{2+}	0.03	0.00	0.00	0.00	0.00	0.00	0.00	0.00
Fe^{2+}	1.51	0.87	0.97	1.18	1.38	1.40	1.31	1.46
Mg	1.88	2.61	2.47	2.29	2.50	2.53	2.36	2.39
Σ*C*	**4.91**	**5.00**	**5.00**	**5.00**	**5.00**	**5.00**	**5.00**	**5.00**
Mn^{2+}	0.00	0.00	0.00	0.01	0.01	0.00	0.01	0.02
Fe^{2+}	0.00	0.23	0.13	0.08	0.13	0.13	0.08	0.08
Ca	1.66	1.35	1.41	1.59	1.74	1.76	1.69	1.82
Na	0.34	0.42	0.47	0.32	0.13	0.10	0.22	0.08

Σ*B*	**2.00**	**2.00**	**2.00**	**2.00**	**2.00**	**2.00**	**2.00**	**2.00**
Na	0.11	0.35	0.26	0.34	0.46	0.45	0.51	0.46
K	0.06	0.05	0.06	0.05	0.05	0.06	0.03	0.06
Σ*A*	**0.17**	**0.40**	**0.33**	**0.38**	**0.50**	**0.51**	**0.54**	**0.51**
Species	***Tsch***	***Tsch***	***Tsch***	***Tsch***	***Prg***	***Prg***	***Prg***	***Prg***

* Total Fe was measured as FeO. FeO/Fe_2O_3 ratio was calculated with ACES_2 Excel spreadsheet (after Locock, 2014).

** H_2O was calculated from the stoichiometry: OH = 2 *apfu*.

Table 4 continued

No.	9	10	11	12	13	14	15
Sample	D05-6	D05	D05	D12	D12	D13	D13
SiO_2	51.86	50.10	51.99	48.05	45.61	46.12	49.49
TiO_2	0.22	0.14	0.23	0.33	0.27	0.23	0.25
Al_2O_3	6.31	8.67	5.47	9.79	13.39	13.04	9.36
MnO	0.37	0.22	0.31	0.19	0.22	0.16	0.14
FeO*	13.24	11.18	13.67	15.09	15.44	13.92	13.04
Fe_2O_3*	0.24	1.40	0.59	2.16	1.93	2.60	1.33
MgO	13.89	13.68	13.50	10.18	8.60	9.76	12.42
CaO	11.50	12.05	11.79	11.30	11.32	11.11	11.22
Na_2O	0.25	0.40	0.33	0.81	1.04	0.87	0.60
K_2O	0.10	0.12	0.08	0.10	0.20	0.18	0.12
H_2O**	2.05	2.04	2.04	2.00	2.00	2.01	2.04
Total	**100.00**	**100.00**	**100.00**	**100.00**	**100.00**	**100.00**	**100.00**
Cation numbers based on 23 oxygens.							
Si	7.45	7.17	7.50	7.03	6.70	6.72	7.13
Al	0.55	0.83	0.50	0.97	1.30	1.28	0.87
Σ*T*	**8.00**	**8.00**	**8.00**	**8.00**	**8.00**	**8.00**	**8.00**
Ti	0.02	0.02	0.02	0.04	0.03	0.03	0.03
Al	0.51	0.64	0.43	0.72	1.01	0.96	0.72
Fe^{3+}	0.03	0.15	0.06	0.24	0.21	0.29	0.14

Mn^{2+}	0.00	0.00	0.00	0.00	0.00	0.00	0.00
Fe^{2+}	1.46	1.28	1.58	1.79	1.86	1.60	1.44
Mg	2.97	2.92	2.90	2.22	1.88	2.12	2.67
Σ*C*	**5.00**	**5.00**	**5.00**	**5.00**	**5.00**	**5.00**	**5.00**
Mn^{2+}	0.05	0.03	0.04	0.02	0.03	0.02	0.02
Fe^{2+}	0.13	0.06	0.07	0.05	0.03	0.09	0.13
Ca	1.77	1.85	1.82	1.77	1.78	1.74	1.73
Na	0.06	0.06	0.07	0.15	0.16	0.15	0.12
Σ*B*	**2.00**	**2.00**	**2.00**	**2.00**	**2.00**	**2.00**	**2.00**
Na	0.01	0.05	0.02	0.08	0.14	0.09	0.05
K	0.02	0.02	0.01	0.02	0.04	0.03	0.02
Σ*A*	**0.03**	**0.07**	**0.04**	**0.10**	**0.17**	**0.13**	**0.07**
Species	***Mg-hb***	***Mg-hb***	***Mg-hb***	***Mg-hb***	***Mg-hb***	***Mg-hb***	***Mg-hb***

Table 5 Chemical composition of amphiboles (*Group 2*).

No.	1	2	3	4	5	6	7	8	9	10
Sample	B12-20	B12-26	B12-31	B12-20	B12-16	B12-17	D17-18	D47-21	D47-22	D47-23
Core/rim										
SiO_2	40.72	40.73	40.35	40.72	41.49	42.34	42.46	39.99	39.48	39.90
TiO_2	0.06	0.45	0.00	0.06	0.16	0.05	0.06	0.60	0.44	0.44
Al_2O_3	19.68	19.07	19.86	19.68	18.06	17.14	15.56	17.52	18.23	18.68
MnO	0.00	0.00	0.05	0.00	0.06	0.00	0.26	0.39	0.45	0.42
FeO*	15.01	14.10	14.00	15.01	14.09	14.33	15.92	16.30	16.72	16.17
Fe_2O_3*	1.55	1.66	1.69	1.55	1.70	1.52	1.44	0.96	1.25	0.74
MgO	7.48	8.35	8.21	7.48	8.77	8.96	8.47	7.75	7.20	7.16
CaO	11.12	10.90	11.00	11.12	11.15	10.92	11.20	10.15	9.99	9.92
Na_2O	2.29	2.60	2.68	2.29	2.30	2.59	2.30	3.31	3.20	3.48
K_2O	0.11	0.15	0.17	0.11	0.23	0.15	0.35	1.07	1.08	1.10
H_2O**	1.99	2.00	2.00	1.99	2.00	2.00	1.98	1.96	1.95	1.97
Total	**100.00**	**100.00**	**100.00**	**100.00**	**100.00**	**100.00**	**100.00**	**100.00**	**100.00**	**100.00**

Cation numbers based on 23 oxygens.										
Si	6.01	6.00	5.94	6.01	6.11	6.23	6.31	6.03	5.98	6.00
Al	2.00	2.01	2.06	2.00	1.89	1.78	1.69	1.97	2.02	2.00
Σ*T*	**8.00**	**8.00**	**8.00**	**8.00**	**8.00**	**8.00**	**8.00**	**8.00**	**8.00**	**8.00**
Ti	0.01	0.05	0.00	0.01	0.02	0.01	0.01	0.07	0.05	0.05
Al	1.42	1.30	1.39	1.42	1.24	1.20	1.04	1.15	1.23	1.31
Fe^{3+}	0.17	0.18	0.19	0.17	0.19	0.17	0.16	0.11	0.14	0.08
Mn^{2+}	0.00	0.00	0.00	0.00	0.00	0.00	0.00	0.00	0.00	0.01
Fe^{2+}	1.75	1.63	1.62	1.75	1.63	1.67	1.92	1.93	1.95	1.95
Mg	1.65	1.83	1.80	1.65	1.92	1.97	1.88	1.74	1.63	1.61
Σ*C*	**5.00**	**5.00**	**5.00**	**5.00**	**5.00**	**5.00**	**5.00**	**5.00**	**5.00**	**5.00**
Mn^{2+}	0.00	0.00	0.01	0.00	0.01	0.00	0.03	0.05	0.06	0.05
Fe^{2+}	0.10	0.11	0.10	0.10	0.10	0.10	0.06	0.01	0.02	0.00
Ca	1.76	1.72	1.74	1.76	1.76	1.72	1.78	1.64	1.62	1.60
Na	0.14	0.18	0.16	0.14	0.13	0.18	0.13	0.30	0.30	0.36
Σ*B*	**2.00**	**2.00**	**2.00**	**2.00**	**2.00**	**2.00**	**2.00**	**2.00**	**2.00**	**2.00**
Na	0.51	0.57	0.61	0.51	0.52	0.56	0.54	0.67	0.64	0.66
K	0.02	0.03	0.03	0.02	0.04	0.03	0.07	0.21	0.21	0.21
Σ*A*	**0.53**	**0.60**	**0.64**	**0.53**	**0.57**	**0.58**	**0.60**	**0.88**	**0.85**	**0.87**
Species	***F-sdg***	***Sdg***	***Sdg***	***F-sdg***	***Prg***	***Prg***	***Fprg***	***Fprg***	***Fprg***	***Fprg***

* Total Fe was measured as FeO. FeO/Fe_2O_3 ratio was calculated with ACES_2 Excel spreadsheet (after Locock, 2014).

** H_2O was calculated from the stoichiometry: OH = 2 *apfu*.

Table 5 continued

No.	11	12	13	14	15	16	17	18	19	20
Sample	D08-5	C02-25	B05-42	D08-29	D15-4	D17-44	C02-11	B05-27	D08-30	D15-2
Core/rim										
SiO_2	40.24	49.72	49.65	47.48	47.19	52.80	50.94	52.89	53.51	52.82
TiO_2	0.00	0.00	0.13	0.08	0.03	0.08	0.03	0.07	0.11	0.00
Al_2O_3	14.28	5.99	8.83	10.88	12.12	5.07	4.87	4.12	4.66	5.06
MnO	0.20	0.14	0.00	0.28	0.09	0.32	0.26	0.00	0.27	0.16
FeO*	18.48	22.82	12.01	10.46	12.51	14.10	20.58	17.83	8.99	9.53
Fe_2O_3*	10.07	0.03	2.50	3.82	1.19	1.00	0.12	0.00	1.09	1.42
MgO	6.73	7.45	12.81	12.65	11.47	13.18	9.23	11.78	17.05	16.03
CaO	7.52	11.64	11.03	11.34	11.64	10.14	11.65	10.83	11.79	12.34
Na_2O	0.25	0.13	0.97	0.85	1.27	1.11	0.21	0.48	0.41	0.54
K_2O	0.23	0.14	0.04	0.15	0.47	0.17	0.12	0.00	0.06	0.05
H_2O**	1.91	1.95	2.03	2.03	2.03	2.04	1.98	2.01	2.07	2.06
Total	**99.91**	**100.00**	**100.00**	**100.00**	**100.00**	**100.00**	**100.00**	**100.00**	**100.00**	**100.00**
Cation numbers based on 23 oxygens.										
Si	6.12	7.47	7.14	6.85	6.83	7.61	7.58	7.71	7.56	7.50
Al	1.88	0.53	0.86	1.15	1.17	0.39	0.42	0.29	0.44	0.50
Σ*T*	**8.00**	**8.00**	**8.00**	**8.00**	**8.00**	**8.00**	**8.00**	**8.00**	**8.00**	**8.00**
Ti	0.00	0.00	0.01	0.01	0.00	0.01	0.00	0.01	0.01	0.00
Al	0.68	0.53	0.64	0.69	0.90	0.47	0.43	0.42	0.33	0.35
Fe^{3+}	1.15	0.00	0.27	0.41	0.13	0.11	0.01	0.00	0.12	0.15
Mn^{2+}	0.00	0.00	0.00	0.00	0.00	0.00	0.00	0.00	0.00	0.00
Fe^{2+}	1.64	2.79	1.33	1.17	1.49	1.58	2.51	2.01	0.95	1.11
Mg	1.53	1.67	2.75	2.72	2.48	2.83	2.05	2.56	3.59	3.39
Σ*C*	**5.00**	**5.00**	**5.00**	**5.00**	**5.00**	**5.00**	**5.00**	**5.00**	**5.00**	**5.00**
Mn^{2+}	0.03	0.02	0.00	0.04	0.01	0.04	0.03	0.00	0.03	0.02
Fe^{2+}	0.71	0.07	0.12	0.10	0.03	0.12	0.05	0.17	0.11	0.02
Ca	1.23	1.87	1.70	1.75	1.81	1.57	1.86	1.69	1.78	1.88

Na	0.04	0.04	0.18	0.12	0.16	0.27	0.06	0.14	0.08	0.08
Σ*B*	**2.00**	**2.00**	**2.00**	**2.00**	**2.00**	**2.00**	**2.00**	**1.99**	**2.00**	**2.00**
Na	0.04	0.00	0.09	0.12	0.20	0.04	0.00	0.00	0.04	0.07
K	0.05	0.03	0.01	0.03	0.09	0.03	0.02	0.00	0.01	0.01
Σ*A*	**0.08**	**0.03**	**0.10**	**0.15**	**0.29**	**0.07**	**0.03**	**0.00**	**0.05**	**0.08**
Species	***F-f-tsch***	***Fhb***	***Mg-hb***	***Mg-hb***	***Mg-hb***	***Mg-hb***	***Fact***	***Act***	***Act***	***Act***

Table 6 Chemical composition of epidotes.

No.	1	2	3	4	5	6	7	8	9	10
Sample	B12	D02	D02	D04	D04	D08	D08	D15	D15	D17
SiO_2	39.52	39.36	39.32	39.13	39.15	38.44	38.83	38.66	39.26	38.83
TiO_2	0.00	0.07	0.46	0.04	0.00	0.00	0.03	0.04	0.08	0.16
Al_2O_3	25.43	26.82	28.95	27.05	29.63	23.82	29.75	27.69	29.52	23.69
Fe_2O_3*	11.04	10.10	7.22	9.52	6.54	13.53	6.72	8.81	6.40	13.24
MnO	0.00	0.00	0.09	0.07	0.00	0.10	0.00	0.06	0.08	0.12
MgO	0.37	0.09	0.07	0.27	0.30	0.17	0.26	0.28	0.41	0.04
CaO	21.46	21.54	21.86	21.79	22.25	21.92	22.37	22.43	21.99	21.95
Na_2O	0.18	0.00	0.00	0.14	0.14	0.06	0.05	0.05	0.25	0.00
K_2O	0.07	0.10	0.09	0.06	0.05	0.06	0.06	0.06	0.07	0.07
H_2O**	1.92	1.92	1.94	1.92	1.94	1.90	1.93	1.92	1.94	1.90
Total	**100.00**	**100.00**	**100.00**	**100.00**	**100.00**	**100.00**	**100.00**	**100.00**	**100.00**	**100.00**
Cation numbers based on 12.5 oxygens.										
Si	3.08	3.06	3.03	3.01	3.01	3.04	2.99	3.00	3.02	3.06
Σ*T*	**3.08**	**3.06**	**3.03**	**3.01**	**3.01**	**3.04**	**2.99**	**3.00**	**3.02**	**3.06**
Ti	0.00	0.00	0.03	0.00	0.00	0.00	0.00	0.00	0.00	0.01
Al	2.34	2.46	2.63	2.45	2.69	2.22	2.69	2.54	2.68	2.20
Fe^{3+}	0.65	0.59	0.42	0.55	0.38	0.80	0.39	0.52	0.37	0.79
Mg	0.00	0.00	0.00	0.00	0.00	0.00	0.00	0.00	0.00	0.00
Σ*M*	**2.99**	**3.05**	**3.08**	**3.00**	**3.07**	**3.02**	**3.08**	**3.06**	**3.05**	**3.00**
Mn^{2+}	0.00	0.00	0.01	0.00	0.00	0.01	0.00	0.00	0.01	0.01

Mg	0.04	0.01	0.01	0.03	0.03	0.02	0.03	0.03	0.05	0.00
Ca	1.79	1.79	1.80	1.80	1.83	1.86	1.85	1.87	1.81	1.86
Na	0.03	0.00	0.00	0.02	0.02	0.01	0.01	0.01	0.04	0.00
K	0.01	0.01	0.01	0.01	0.00	0.01	0.01	0.01	0.01	0.01
Σ*A*	**1.87**	**1.81**	**1.83**	**1.86**	**1.88**	**1.91**	**1.90**	**1.92**	**1.92**	**1.88**
Species	***Ep***	***Ep***	***Czo***	***Ep***	***Czo***	***Ep***	***Czo***	***Ep***	***Czo***	***Ep***

* Total Fe was measured as Fe_2O_3.

** H_2O was calculated from the stoichiometry: OH = 1 *apfu*.

Table 7 Chemical composition of biotites.

No.	1	2	3	4
Sample	D15	D17	D17	D17
SiO_2	39.72	38.09	39.79	39.06
TiO_2	0.17	0.22	0.15	0.15
Al_2O_3	16.42	18.55	16.70	17.45
FeO*	14.49	14.18	13.20	13.33
MnO	0.06	0.12	0.12	0.10
MgO	15.59	15.19	16.24	16.38
CaO	0.50	0.11	0.15	0.17
Na_2O	0.20	0.06	0.00	0.00
K_2O	8.75	9.39	9.52	9.25
H_2O**	4.10	4.10	4.11	4.11
Total	100.00	100.00	100.00	100.00
Cation numbers based on 11 oxygens				
Si	2.90	2.79	2.90	2.85
Al	1.10	1.21	1.10	1.15
Σ*T*	**4.00**	**4.00**	**4.00**	**4.00**
Al	0.32	0.39	0.33	0.35
Ti	0.01	0.01	0.01	0.01

Fe^{2+}	0.89	0.87	0.81	0.81
Mn	0.00	0.01	0.01	0.01
Mg	1.70	1.66	1.77	1.78
ΣM	**2.92**	**2.95**	**2.93**	**2.96**
Ca	0.04	0.01	0.01	0.01
Na	0.03	0.01	0.00	0.00
K	0.82	0.88	0.89	0.86
Σ*I*	**0.88**	**0.90**	**0.90**	**0.87**

* Total Fe was measured as FeO.

** H_2O was calculated from the stoichiometry: OH = 2 *apfu*.

Table 8 Chemical composition of chlorites.

No.	1	2	3	4	5	6	7	8	9	10
Sample	D13	D13	C02	C02	D04	D02	D02	D21	D21	D21
SiO_2	27.77	30.38	29.69	29.63	27.12	27.84	29.99	20.88	20.33	24.52
TiO_2	0.13	0.07	0.04	0.09	0.02	0.04	0.00	0.00	0.00	0.00
Al_2O_3	21.63	20.36	18.72	18.98	20.66	19.91	20.22	13.31	16.19	15.24
Fe_2O_3*	0.00	0.00	0.00	0.00	0.00	0.00	0.00	13.29	13.07	4.90
FeO*	20.68	19.87	26.95	26.37	37.45	29.04	28.14	39.53	34.52	39.39
MnO	0.08	0.13	0.35	0.30	0.12	0.20	0.08	0.08	0.00	0.00
MgO	17.65	15.41	11.52	12.21	3.44	11.57	10.03	2.55	5.27	4.74
CaO	0.20	1.64	1.20	0.79	0.25	0.00	0.00	0.13	0.05	0.25
Na_2O	0.03	0.22	0.00	0.00	0.00	0.00	0.00	0.13	0.19	0.32
K_2O	0.02	0.04	0.07	0.12	0.00	0.03	0.03	0.04	0.02	0.19
H_2O**	11.82	11.87	11.47	11.51	10.93	11.37	11.51	10.07	10.36	10.46
Total	**100.00**	**100.00**	**100.00**	**100.00**	**100.00**	**100.00**	**100.00**	**100.00**	**100.00**	**100.00**
Cation numbers based on 14 oxygens.										
Si	2.82	3.07	3.11	3.09	2.98	2.94	3.13	2.49	2.35	2.81
Al	1.18	0.93	0.89	0.91	1.02	1.06	0.87	1.51	1.65	1.19
Σ*T*	**4.00**	**4.00**	**4.00**	**4.00**	**4.00**	**4.00**	**4.00**	**4.00**	**4.00**	**4.00**

Al	1.41	1.49	1.41	1.42	1.65	1.41	1.61	0.36	0.56	0.87
Ti	0.01	0.01	0.00	0.01	0.00	0.00	0.00	0.00	0.00	0.00
Fe^{3+}	0.00	0.00	0.00	0.00	0.00	0.00	0.00	1.19	1.14	0.42
Fe^{2+}	1.76	1.68	2.36	2.30	3.44	2.56	2.45	3.93	3.34	3.77
Mn	0.01	0.01	0.03	0.03	0.01	0.02	0.01	0.01	0.00	0.00
Mg	2.67	2.32	1.80	1.90	0.56	1.82	1.56	0.45	0.91	0.81
Ca	0.02	0.18	0.13	0.09	0.03	0.00	0.00	0.02	0.01	0.03
Na	0.01	0.04	0.00	0.00	0.00	0.00	0.00	0.03	0.04	0.07
K	0.00	0.01	0.01	0.02	0.00	0.00	0.00	0.01	0.00	0.03
Σ*M*	**5.88**	**5.74**	**5.74**	**5.75**	**5.69**	**5.82**	**5.63**	**6.00**	**6.00**	**6.00**

* Total Fe was measured as FeO. FeO/Fe_2O_3 ratio was calculated from the stoichiometry: Σ*M* = 6.00 *apfu*.

** H_2O was calculated from the stoichiometry: OH = 8 *apfu*.

Table 9

Thermobarometry data of polished stone tools. MT: Medium-temperature amphibolites; HT: High-temperature amphibolites. *: measured with “original-surface” method.

Sample	**Number of measurements**	**T_{avg} (°C)**	**P_{avg} (kbar)**	**Standard deviation T (°C)**	**Standard deviation P (kbar)**	**T_{max} (°C)**	**$P_{(Tmax)}$ (kbar)**
MT							
B04	2	441	2.7	8.49	0.12	450	2.8
B05	3	510	3.9	7.58	0.17	516	4.0
C02	4	442	2.7	12.88	0.18	450	2.8
D02	2	480	3.4	22.45	0.41	500	3.7
D04	1	510	3.7	0.00	0.00	510	3.7
D05	1	540	5.3	0.00	0.00	540	5.3
D09	3	480	3.0	28.36	0.38	510	3.5
D18	3	530	4.0	14.32	0.18	545	4.1
D21	8	540	2.8	18.66	0.18	600	3.4
D32*	1	548	4.0	0.00	0.00	548	4.0
D33*	3	455	2.7	9.73	0.21	460	2.8
HT							
B12	6	670	7.1	12.53	0.30	680	7.3
D08	6	580	4.7	38.66	0.55	600	4.8
D12	3	540	4.7	25.75	0.59	570	5.0
D13	5	520	4.0	28.14	0.56	560	5.0

D15	1	555	4.8	0.00	0.00	555	4.8
D17	1	610	5.7	0.00	0.00	610	5.7
D31*	13	620	5.7	12.94	0.35	635	6.2
D30*	16	588	5.1	21.55	0.48	612	5.6
D34*	6	550	4.5	20.71	0.37	580	5.1
D47*	6	630	6.0	61.46	1.18	690	7.0
D48*	5	580	4.7	7.73	0.08	590	4.60

Table 10

Amphibolite stone implements and their possible provenance fields.
(Abbreviations: G1: *Group1*, G2a: *Group2a*, G2b: *Group2b*, G2c: *Group2c*, G2d: *Group2d*).

*** the most likely, ** likely, * possible

Possible provenance fields/Samples	D05-G1	D12-G1	D13-G1	D30-G1	D31-G1	D33-G1	B12-G2a	D02-G2a	D04-G2a	D08-G2a	D18-G2a
Gemericum											
Klátov				***	***		**	**	**	*	*
Gemericum-Veporicum											
Ochtiná group	***	***	***	**	**	**		**	**	*	*
Veporicum	*	*	*	*	*	*					
Branisko										*	*
Čierna Hora						**					*
Čierny Balog											
Tatricum	*	*	*	*	*	*					
Little Carpathians									*	*	*
Tribeč											
Stražovské Mountains										*	
Zemplinicum							**				

Table 10 continued

Possible provenance fields/Samples	D21-G2a	D32-G2a	D47-G2a	B04-G2b	B05-G2b	C02-G2b	D48-G2b	D15-G2c	D34-G2c	D45-G2c	D17-G2d
Gemericum											
Klátov	*	*	**				*	***	***	***	**
Gemericum-Veporicum											
Ochtiná group	*	*					*				
Veporicum											
Branisko	*	*		**	**	**	**	*	*	*	
Čierna Hora	*	*		***	***	***		*	*	*	
Čierny Balog											
Tatricum											

Little Carpathians	*	*				*		*	*	*	
Tribeč											
Stražovské Mountains											
Zemplinicum			**								

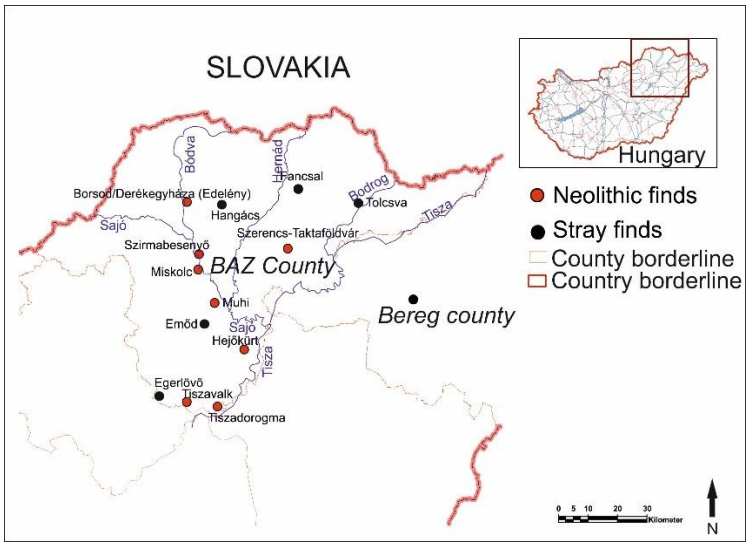

Figure 1

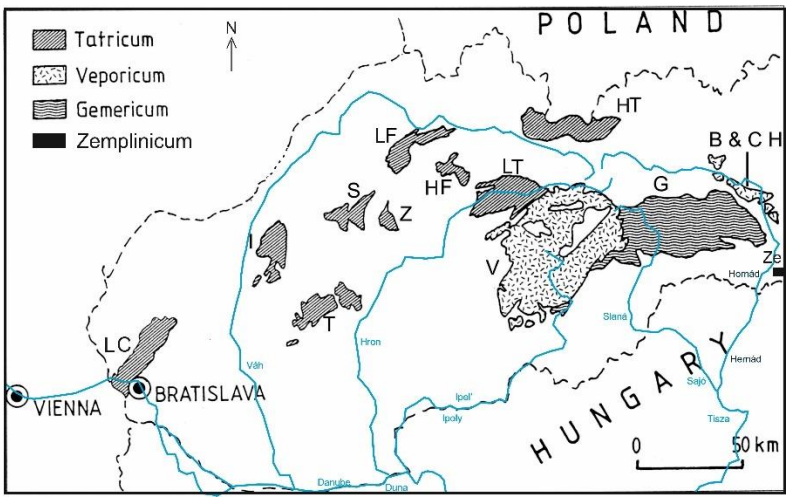

Figure 2

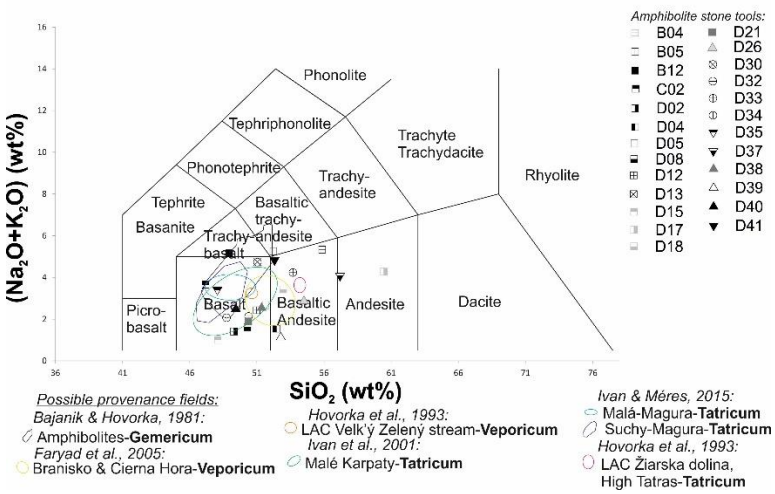

Figure 3

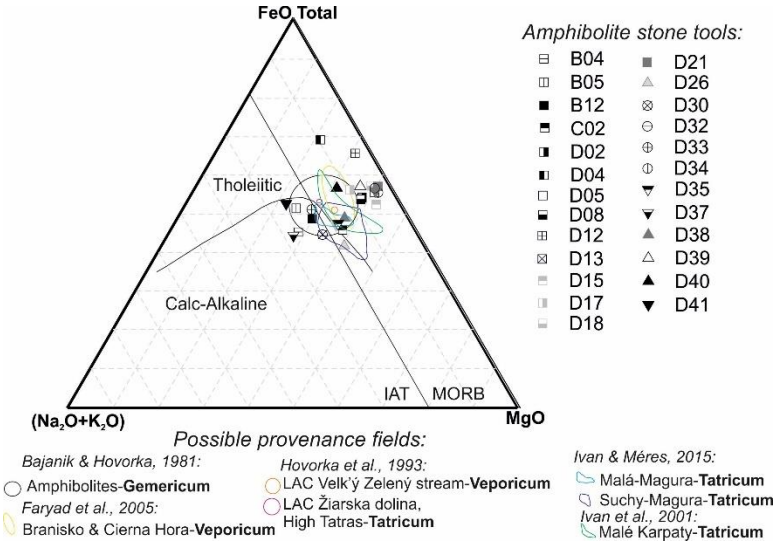

Figure 4

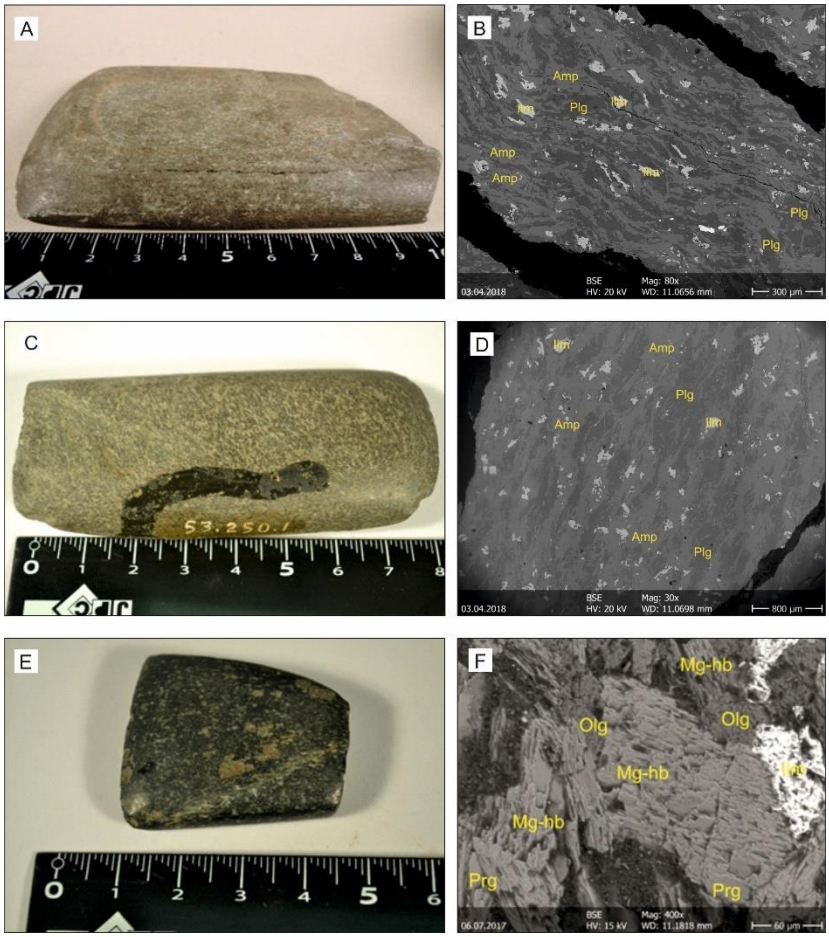
A
B
Amp
Plg
Ilm
Amp
Amp
Plg
Plg
BSE
HV: 20 kV
Mag: 80x
WD: 11.0656 mm
300 µm
C
53.250.1
D
Ilm
Amp
Plg
Amp
Ilm
Amp
Plg
03.04.2018
BSE
HV: 20 kV
Mag: 30x
WD: 11.0698 mm
800 µm
E
F
Mg-hb
Olg
Olg
Mg-hb
Ilm
Mg-hb
Prg
Prg
06.07.2017
BSE
HV: 15 kV
Mag: 400x
WD: 11.1818 mm
60 µm

Figure 5

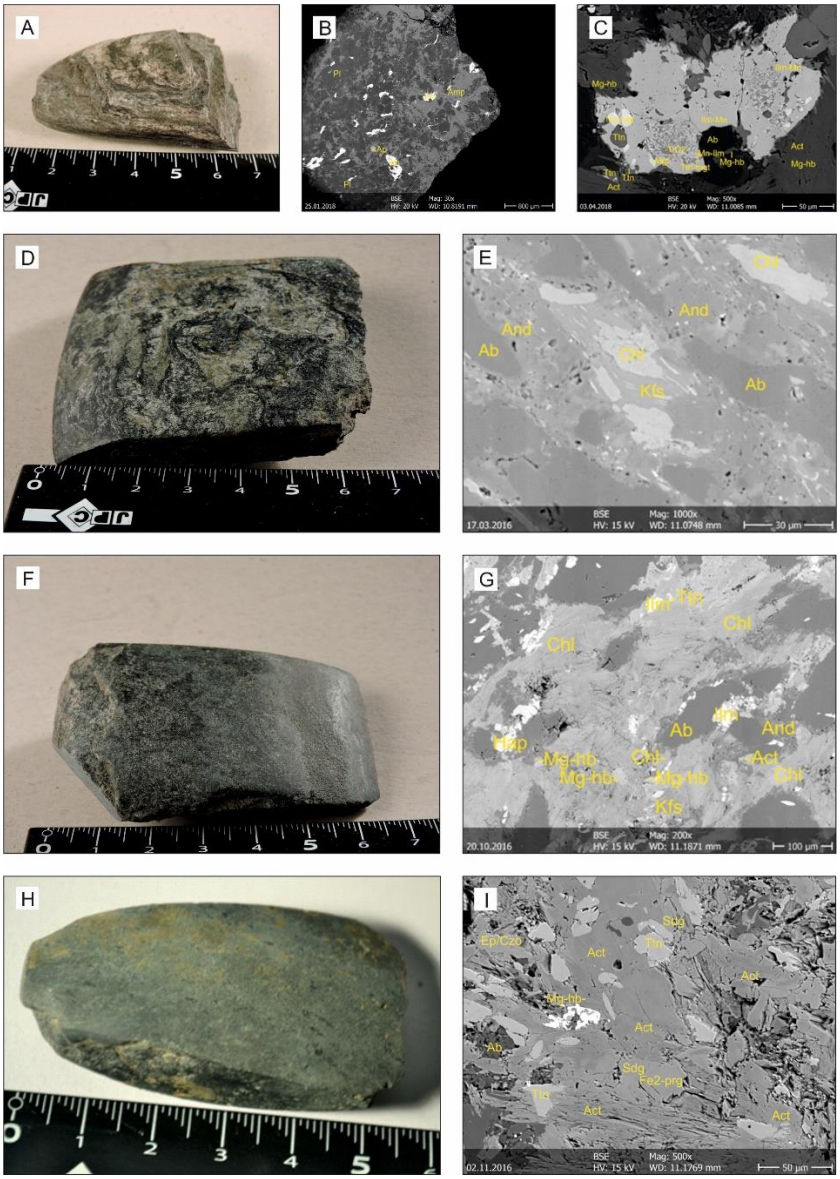
A
B
Pl
Amp
Ap
Pl
C
Mg-hb
Tlm
Ab
Act
Mg-hb
Act
D
E
Chl
And
And
Ab
Chl
Kfs
Ab
17.03.2016
BSE
Mag: 1000x
HV: 15 kV
WD: 11.0748 mm
30 µm
F
G
Ilm?
Tlm
Chl
Chl
Ab
Ilm
And
Ttn
Mg-hb
Chl
Act
Mg-hb
Mg-hb
Chl
Kfs
20.10.2016
BSE
Mag: 200x
HV: 15 kV
WD: 11.1871 mm
100 µm
H
I
Sdg
Ep/Czo
Act
Tlm
Act
Mg-hb
Act
Ab
Sdg
Fe2-prg
Tlm
Act
Act
02.11.2016
BSE
Mag: 500x
HV: 15 kV
WD: 11.1769 mm
50 µm

Figure 6

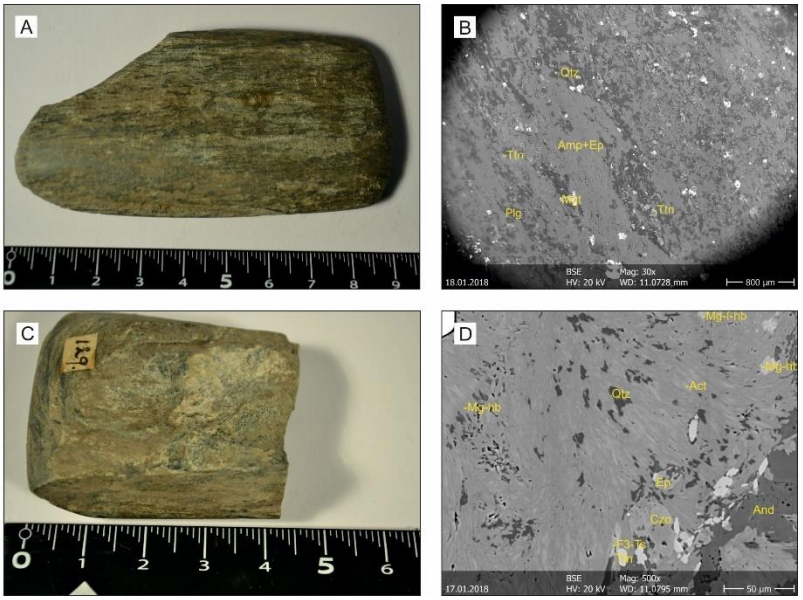

Figure 7

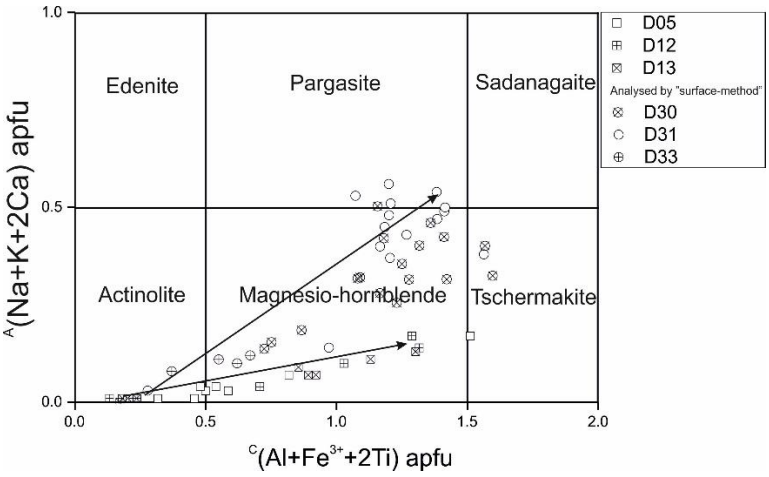

Figure 8

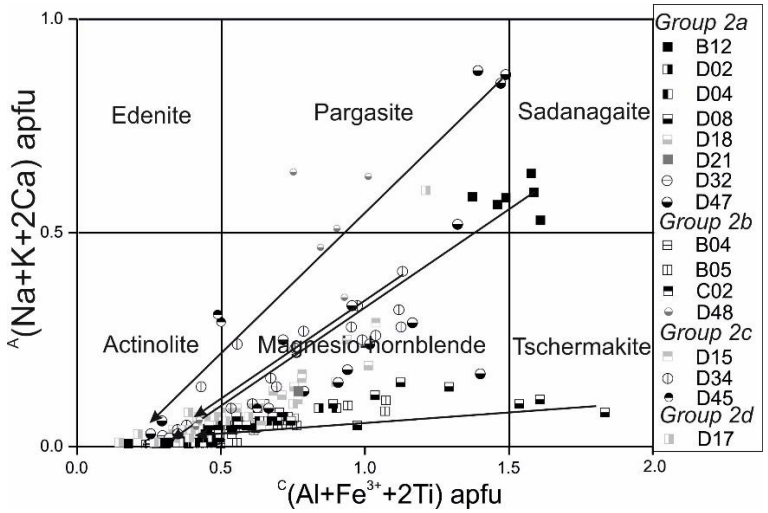

Figure 9